Technical Note

1977-29

R. J. Becherer

System Design Study for Infrared Airborne Radar (IRAR)

18 October 1977

Prepared for the Department of the Air Force
under Electronic Systems Division Contract F19628-78-C-0002 by

Lincoln Laboratory
MASSACHUSETTS INSTITUTE OF TECHNOLOGY
LEXINGTON, MASSACHUSETTS

The work reported in this document was performed at Lincoln Laboratory, a center for research operated by Massachusetts Institute of Technology, with the support of the Department of the Air Force under Contract F19628-78-C-0002.

This technical report has been reviewed and is approved for publication.

FOR THE COMMANDER

Raymond L. Loiselle

Raymond L. Loiselle, Lt. Col., USAF
Chief, ESD Lincoln Laboratory Project Office

MASSACHUSETTS INSTITUTE OF TECHNOLOGY

LINCOLN LABORATORY

SYSTEM DESIGN STUDY FOR INFRARED AIRBORNE RADAR (IRAR)

R. J. BECHERER

Group 53

TECHNICAL NOTE 1977-29

18 OCTOBER 1977

LEXINGTON MASSACHUSETTS

ABSTRACT

This technical note describes the design of a tactical near-all-weather infrared airborne radar (IRAR). The requirements for this radar include both (1) wide field MTI search for target detection against a cluttered terrain background and (2) narrow field high angular resolution imagery for target recognition and identification.

The principal new technology issues identified and techniques proposed include a heterodyne detection antenna/receiver in an array configuration, compact Maksutov-Cassegrain telescope optics design, MTI pulse integration signal processing, and real time image processing for speckle and glint reduction.

Expected weather penetration capability for this radar is assessed with the aid of a recent analysis of real weather data from a number of locations in Central Europe.

TABLE OF CONTENTS

I. INTRODUCTION

Studies of the air-to-ground tactical mission have led to the conclusion that a real need exists for a high angular resolution imaging sensor which will be capable of near-all-weather operation at the relatively short ranges associated with this mission.

There are several general requirements which should be met by such a sensor. It should be compact, lightweight, and achieve minimum cost in quantity. It should provide angular resolution adequate for classification and identification. It should also provide a capability for wide field search with high detection probability. In the high resolution imaging mode it should operate at frame rates or data rates compatible with the low altitude high velocity tactical geometry. In the search mode it should provide scan rates compatible with aircraft forward motion. Finally, the sensor should perform adequately under a variety of weather conditions so that, in effect, air-to-ground operations are not restricted by sensor capability.

This technical note begins with an analysis of the real mission needs and their impact on sensor system requirements. An examination of the requirements suggests that an infrared imaging laser radar is a promising candidate which should be evaluated. This evaluation is then conducted to define the associated component technology requirements.

In addition to identifying technology issues, we propose certain techniques which will provide the required performance. These include compact telescope optics, a design concept for an infrared heterodyne

antenna/receiver which operates in an array configuration, and MTI pulse signal processing methods which lower the velocity detection threshold and/or increase weather penetration.

The evaluation of this candidate sensor makes use of imaging signal-to-noise ratio (SNR) calculations. These calculations are combined with recent statistical analyses of real weather data from a number of locations in central Europe. This permits a realistic determination of the expected operational utility, or the fraction of the time when the sensor will not be limited by weather. To establish some basis for comparison we also determine the operational utility for a high quality state-of-the-art FLIR and the expected operational utility of an advanced generation FLIR design which would employ a large CCD or CID focal plane of 10^4 detector elements.

To provide an outline then of the following sections, section 2 (operating modes) addresses the sensor requirements based on mission needs, sections 3-5 (optics, heterodyne array antenna/receiver, and MTI detection and signal processing) present proposed technology developments and designs to meet the sensor requirements, section 6 (image SNR) introduces the calculations required to evaluate sensor performance, section 7 (image processing) evaluates processing requirements, and finally section 8 (system performance under varying weather conditions) presents the evaluation of expected operational utility, or fraction of time operating, under the weather conditions of central Europe for the state-of-the-art FLIR, the CCD/CID FLIR, and the tactical infrared airborne radar. For the Infra-Red Airborne Radar we use the acronym IRAR.

II. OPERATING MODES

The primary sensor requirement in the air-to-ground tactical mission is for target acquisition. There are two types of acquisition. One is the detection and general location of some objects of possible military interest from remote stand-off platforms. This type of acquisition is important and useful but is not of interest here. The second type of acquisition, and the type of concern here, is real-time short-range detection, recognition, and identification from a low-flying high velocity tactical aircraft.

Detection, recognition, and identification are then the three phases of real time target acquisition. Detection refers to the location of an object of military interest within a relatively wide search field-of-view (FOV). Recognition refers to the classification of a detected object as being for example a truck, a tank, or some other type of vehicle. Identification refers to a higher degree of classification of the object as being, for example, a T-62 type tank. Detection then involves a wide FOV while recognition and identification require high spatial resolution but only a narrow FOV.

a. Wide Field Search for Detection

Effective detection implies some discrimination mechanism to separate objects of interest from background or "clutter". The temperature or emissivity difference between a hot object and its background provides this discrimination mechanism in a passive thermal sensor[1]. In an active sensor which has a coherent detection capability it has been found that moving

target indication (MTI) based on the doppler effect is an extremely effective technique for discrimination[2]. An MTI detector is characterized by the minimum radial velocity which can be detected. For an effective tactical search sensor this threshold velocity should be lower than a few miles or km per hour. In addition to this threshold velocity requirement it is necessary that the sensor operate over a relatively wide FOV to detect moving objects over a wide swath ahead of the moving aircraft.

Consider the geometry shown in Figure 1. An aircraft carrying a line scan search sensor flies at velocity v and altitude h. The sensor scans the ground in the azimuth direction at a slant range R ahead of the aircraft. Coverage in the forward direction is provided by the forward motion of the aircraft. In order to provide continuous coverage of the ground the azimuth scan rate must be adequate to complete one full azimuth scan by the time the aircraft has moved one beam width in the forward direction.

The projected beam width on the ground in the forward direction is found from Figure 1 to be $\alpha h/\cos^2\beta$ where α is the angular beam size. The time required for the aircraft forward velocity v to move the beam this distance in the forward direction is $t_A = \alpha h/v \cos^2\beta$. Each azimuth scan must therefore be completed in this time. Within each azimuth scan there are $N = FOV/\alpha$ beam widths. We can then determine that the dwell time of the sensor on each angular resolution element on the ground is $t_D = t_A/N$ or, using $\cos\beta = h/R$,

$$t_D = \frac{\alpha^2 R^2}{v\ h\ (FOV)} \tag{1}$$

where

α = angular beam width

FOV = azimuth scan field of view

v = aircraft velocity

h = aircraft altitude

and the associated requirement for bandwidth is at least $B = 1/t_D$.

The angular rate required for the azimuth optical scanner in this sensor is then $\dot{\phi} = FOV/t_A$ or

$$\dot{\phi} = \frac{v\ h\ (FOV)}{\alpha\ R^2} \tag{2}$$

It should be noted that if the search sensor employed a linear array of n detectors arranged to cover a number of resolution elements in the forward direction then the required azimuth scan rate $\dot{\phi}$ would be reduced by the factor n and the dwell time t_D on each resolution element would be increased by the factor n. In an active system the transmitted beam would also have to be fanned out to cover a corresponding number of resolution elements.

Figure 2 shows the bandwidth B and azimuth scan rate $\dot{\phi}$ obtained from (1) and (2) for some typical parameters and also shows the significant reduction in bandwidth and scan rate which can be realized by using a

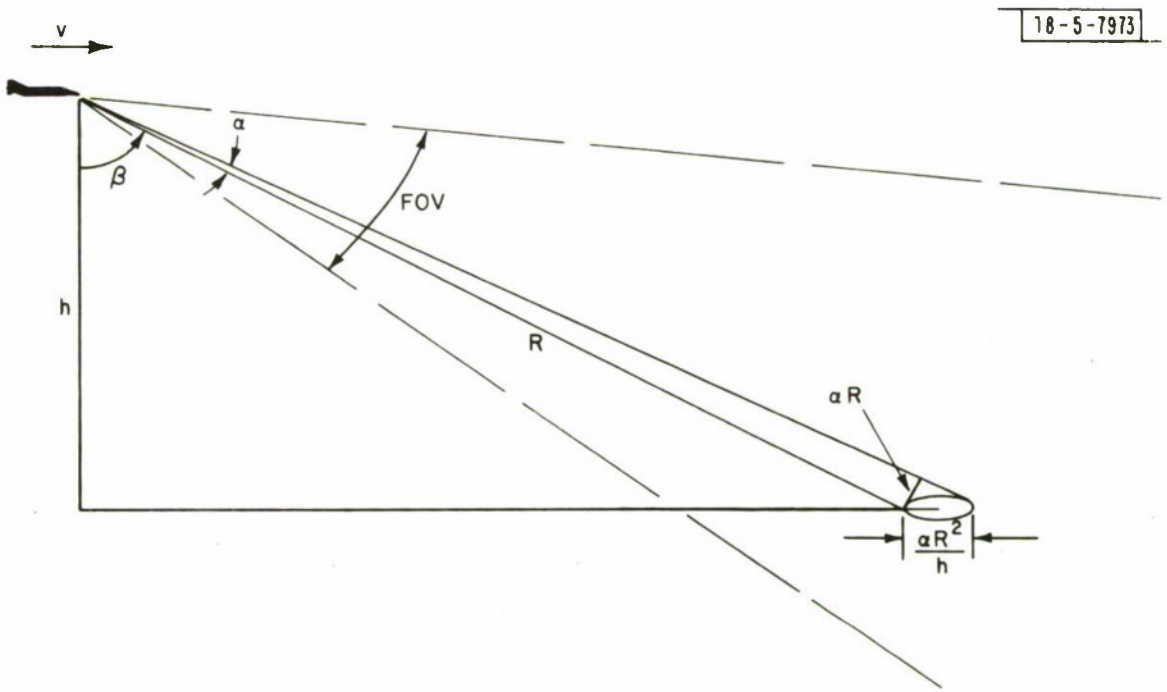

Fig. 1. Tactical aircraft search geometry.

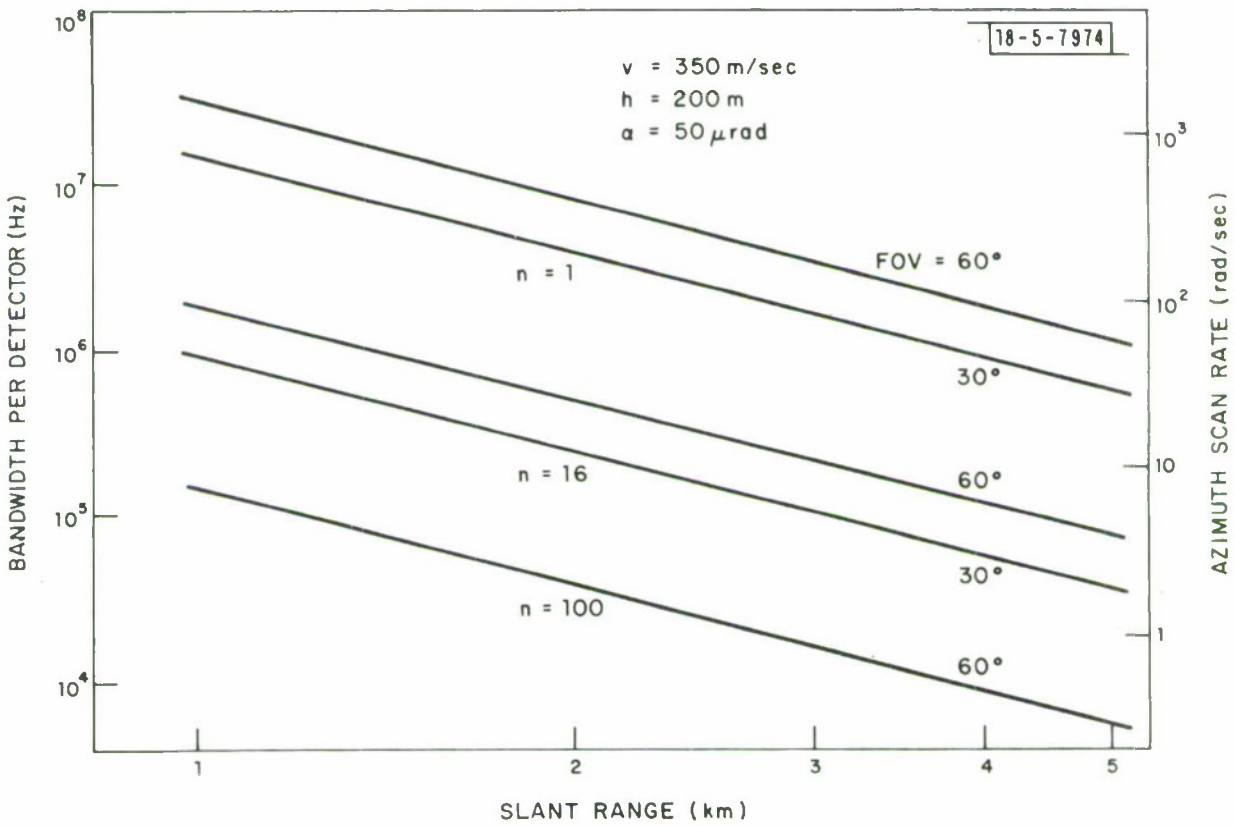

Fig. 2. Bandwidth and azimuth scan rate requirements in wide field search mode.

linear array of detectors with n = 16 or n = 100. As a result of the bandwidth reduction the noise in each detector will be reduced. In a passive thermal sensor this reduction of noise will increase the SNR as $\sqrt{B}$. However, in an active coherent system the associated requirement of fanning the power of the transmitted beam to cover all n resolution elements just offsets this noise reduction so that there is no net change is SNR when compared with n = 1.

A very important consequence of using detector arrays in either the active or passive sensor is that the azimuth scan rate is reduced. Mechanical scanning of an aperture which is typically 10-20 cm in diameter to cover a 30-60^{o} FOV would be very difficult at $\dot{\phi}$ = 100 rad/sec. Scan rates between 1-5 rad/sec are, however, feasible within the limits of current technology.

Some of the mission factors which determine the actual FOV requirements are target mobility relative to aircraft mobility, terrain masking, and reaction time. If the ratio of target speed to aircraft is $v_T/v = 1/20$, for example, then during the time it takes an aircraft to fly 40 km to reach the target, the mobile target can have moved 2 km. Thus, information on the location of mobile targets can become old very quickly. This generates one requirement for a wide search FOV.

Terrain masking is a serious limitation for low flying aircraft. The roughness of the terrain ahead of the aircraft limits its ability to sense targets. In almost all areas of central Europe, terrain masking limits the sensor range to something less than 5 km. In some terrain the limit

can be much less than 5 km, but in considering sensor design capability the larger figures should be used to permit operation in almost all terrain.

Reaction time for the aircraft is also a factor. Detection must take place at long enough ranges to insure that adequate time remains for reacting to the detection, including the time required for identification in the narrow field imaging mode. An aircraft flying at v = 0.5 Mach covers 1 km in 6 seconds. Detection must then take place at ranges of 2-5 km. Taking 3 km as a typical slant range for the search sensor, the 30^{o} and 60^{o} FOV would cover a swath either 1.5 or 3 km wide ahead of the aircraft. This swath coverage is consistent with the target mobility example given above.

In summary then the mission requirements for wide field search for detection lead to FOV, azimuth scan rate, and bandwidth requirements. The azimuth scan rates associated with high angular resolution (small α) indicate the need for arrays of detectors to enable the search sensor to cover a wide FOV. Bandwidth requirements for each detector are in the range 10^{4} - 10^{7} Hz depending strongly on number of detectors and slant range during search but not strongly on small FOV changes. Finally, an effective discriminant of targets from background is essential. In section 5 we examine MTI detection in this role. The advantage of using a high angular resolution sensor in the search mode will then be apparent.

b. Narrow Field Imaging for Identification

Having considered the system requirements associated with wide field search for detection, we now consider the additional requirements associated

with narrow field imaging for recognition and identification. We are assuming that the combined requirements will lead to a single sensor which is usable in either mode.

High angular or spatial resolution is essential for identification. This resolution must be provided while maintaining adequate image SNR. Simulations of tactical imagery[3] indicate that in situations where the displayed image is limited by resolution rather than SNR, recognition requires approximately 8 resolution elements across the minimum dimension of the target and identification requires approximately 13. These values provide a basis for estimating the sensor angular resolution required for identification of typical targets at various slant ranges.

To provide this estimate we take the angular resolution to be λ/D where λ is the wavelength and D the sensor aperture diameter. The number of resolution elements across a minimum dimension h at slant range R is then $hD/\lambda R$ so that required sensor diameter for recognition or identification is

$$D_R = \begin{cases} 8\ \lambda R/h & \text{recognition} \\ 13\ \lambda R/h & \text{identification} \end{cases} \qquad (3)$$

For a typical target, a tank, the minimum dimension is the height and $h \tilde{=} 2$ meters. For $\lambda = 10\mu m$ in the middle of the long wave IR atmospheric window the required diameter D_R is as shown in Figure 3.

The figure shows that at 3 km the aperture diameter required for identification is approximately 20 cm. The 3 km slant range is a typical

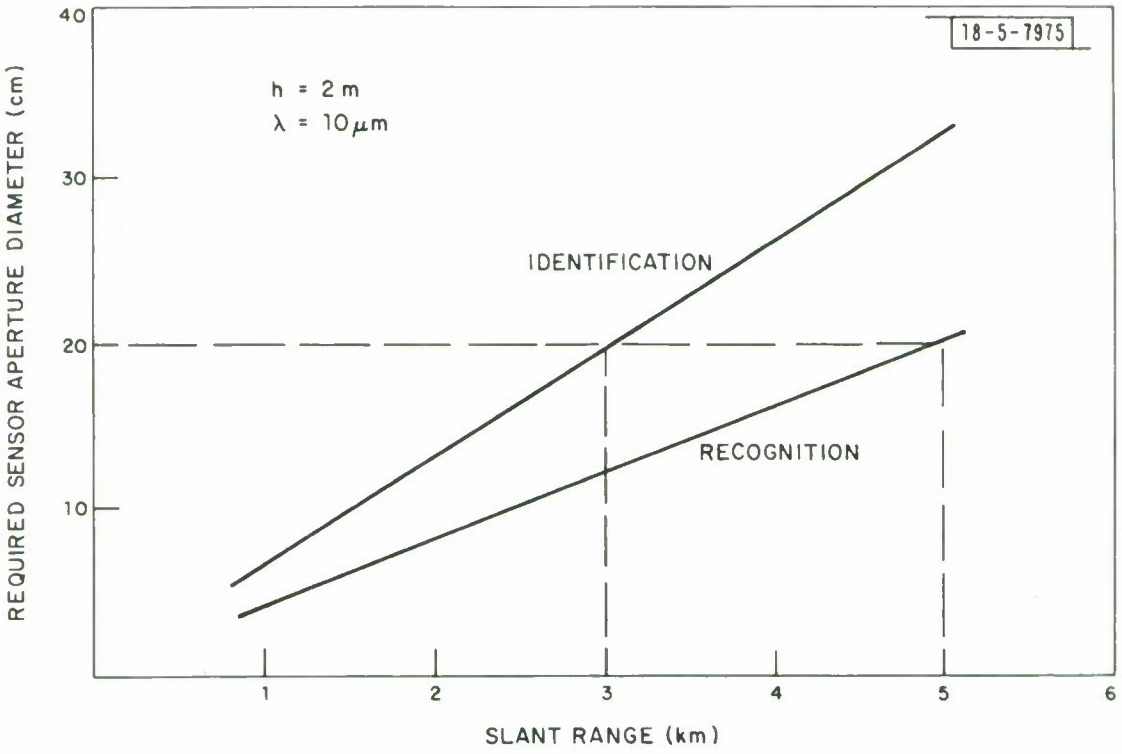

Fig. 3. Sensor aperture diameter required for target recognition and identification.

maximum range at which the sensor would have detected a possible target and been switched to the narrow FOV high resolution imaging mode. With a 20 cm aperture the resolution is then adequate for identification at all ranges less than 3 km and for recognition at ranges out to 5 km. These estimates have not considered the effects of atmospheric turbulence or sensor pointing stability and these issues should also be addressed.

In addition to angular resolution, identification also requires high frame rates and adequate FOV to cover the target. These are two reasons for a high frame rate requirement. The first is that the human visual system bandwidth should limit the information rate. The human visual system has an information bandwidth[4] of approximately 5-10 Hz but detects flicker in imagery presented at less than 30 Hz. If a frame rate of 30 Hz is used then both visual system requirements are satisfied.

The second reason is that the low-altitude high-speed tactical aircraft geometry is changing rapidly. Tracking and stabilizing the target imagery under these changing conditions requires high frame rates.

The FOV in the high resolution identification mode must more than cover the largest dimension of the target at the shortest range. Figure 4 shows the FOV which will include the tank of 6 meters length, a typical maximum tank dimension. The FOV required increases rapidly as the range decreases. The actual FOV should be somewhat larger than the minimum requirement shown in Figure 4 to facilitate tracking and to use contrast

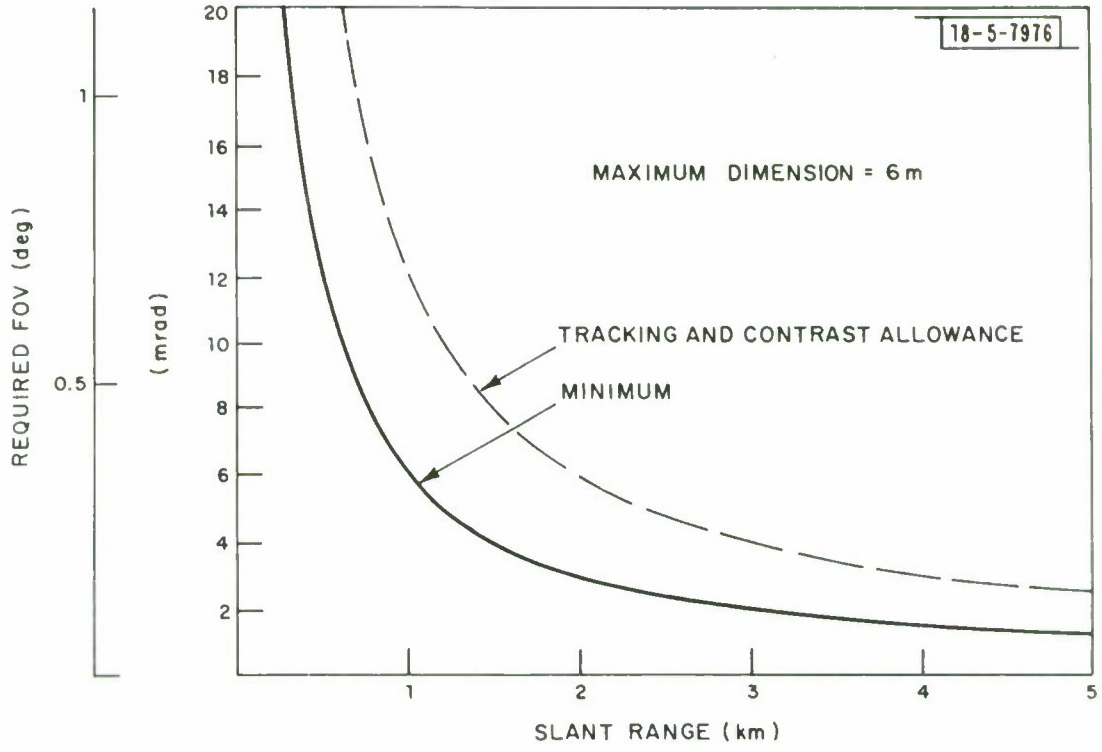

Fig. 4. FOV requirement in narrow field imaging for identification.

between target and background as an aid to identification. Figure 4 shows a dotted curve to indicate the FOV which would be twice as large as the minimum. A minimum FOV requirement for target identification would be approximately 6 mr if the minimum range is taken to be 1 km. A more desirable FOV of 24 mr or 1.4^{o} would allow for tracking and contrast utilization at ranges down to 500 meters.

The FOV required for target identification is small enough so that image space scanning can be utilized. Since the telescope beam size is reduced in image space it is possible to use a much smaller scanner than would be required otherwise. This reduction of scanner size is essential for operation at 30 frames/second or higher frame rates.

Having examined the frame rate and FOV requirements we now consider their combined effect on system bandwidth in the narrow field high resolution identification mode. If the signal from the target is sampled once for each spatial resolution element scanned then the signal bandwidth requirement is

$$B = \frac{\dot{F}\ (FOV)^2}{\theta^2} \tag{4}$$

where $\dot{F}$ is the frame rate, FOV is the field-of-view, and θ is the angular resolution element. For simplicity we have assumed in (4) that the image format is square. This bandwidth requirement is shown in Figure 5 as a function of FOV. As in the wide field search mode the use of detector arrays of n elements will reduce the bandwidth requirement by the factor n.

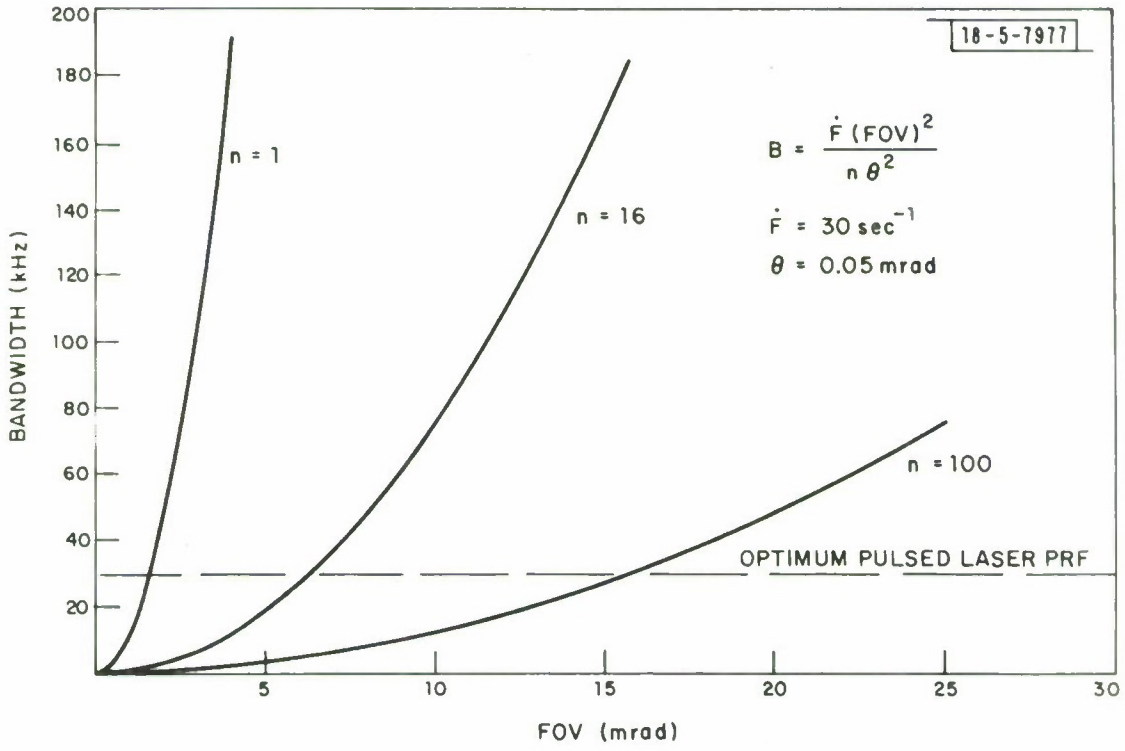

Fig. 5. Narrow field imaging bandwidth showing dependence on FOV and on number of detectors n.

This is also shown in the figure.

Bandwidth reduction is important in the narrow field imaging mode for the following reason. An active sensor operating in the high resolution imaging mode can utilize range-to-target data. This data can be provided by using a pulsed laser transmitter. The pulsed laser PRF should be high enough to achieve maximum average laser power but low enough to provide unambiguous range data out to 5 km. The optimum is then approximately 30 kHz. Obviously, the bandwidth given in (4) can be no greater than the PRF of the laser. When arrays of detectors are used to reduce the bandwidth B it then becomes possible to operate at higher frame rates and/or over larger FOV's than would otherwise be possible. Figure 5 shows that with n = 16 it is just possible to achieve FOV = 6 mr, the minimum required at 1 km in Figure 4.

In the following section we address the question of optical design for a compact, lightweight telescope of 20 cm aperture capable of operation over the field-of-view required. The implementation of detector array concepts is then described in section 4.

III. OPTICS

In this section we consider candidate designs to meet the optical telescope requirements. The requirements include those associated with high resolution identification as well as those for wide field search. A suitable design must therefore provide the aperture diameter and identification FOV defined in section IIb as well as meet the azimuth scan

rate requirements defined in section 2a. The resolution should be essentially diffraction limited. The design should also be as compact and lightweight as possible and should be reproducible at minimum cost in quantity.

The requirement for both compactness and lightweight for 20 cm aperture being considered here indicates that the telescope should be a Cassegrain reflecting design of low f/no. Unfortunately, reflecting elements provide less opportunity for aberration balancing and correction over the required FOV than would be the case with the refracting design. This can be partially offset by using reflecting surfaces for the elements of large diameter and employing some small refracting or reflecting elements after the beam size has been reduced to remove residual aberrations. Also, reducing the f/no increases the aberrations, particularly spherical and coma, so that some compromise may be required.

Table 1 shows a list of candidate optical telescope configurations. The table also shows the shape of the primary and secondary reflecting surfaces for each configuration. The basic principle employed in the design of the first two systems, the Dall-Kirkham and the classical Cassegrain is that a paraboloidal primary reflector provides geometrically perfect imagery on axis for a distant point source. Unfortunately, the image quality for points off axis degrades rapidly with distance from the axis and the secondary mirror is intended to partially correct the resulting coma. In the case of the Classical Cassegrain this is done with some success by using a hyperboloidal secondary which is however expensive to

TABLE 1

CANDIDATE OPTICAL SYSTEM CONFIGURATIONS

CANDIDATE REFLECTING TELESCOPE CONFIGURATIONS	PRIMARY AND SECONDARY SURFACE SHAPE	UNIQUE FEATURES	DOMINANT RESIDUAL ABERRATION
Dall-Kirkham	Primary-Ellipsoidal* Secondary-Spherical	Secondary Fabrication Simple	Coma
Classical Cassegrain	Primary-Paraboloid Secondary-Hyperboloid	Secondary Fabrication Expensive	Coma
Ritchey-Chretien	Primary-Hyperboloid Secondary-Hyperboloid	Secondary Fabrication Expensive	Astigmatism and Petzval Field Curvature
Schmidt	Primary-Spherical Secondary-None	Aspheric Corrector Plate-Expensive	Curved Focal Plane
Maksutov	Primary-Spherical Secondary-None	Spherical Meniscus Corrector Plate	Curved Focal Plane, Small Residual Spherical
Maksutov-Cassegrain	Primary-Spherical Secondary-None	All Spherical Surfaces, Compact	Curved Focal Plane, Small Residual Spherical

*(Under-Corrected Paraboloid)

fabricate. The Dall-Kirkham eliminates the expensive hyperboloidal secondary by replacing it with a simple spherical surface and by under correcting the paraboloidal primary to produce an ellipsoid. This results in some loss of image quality. Both systems are still limited by residual coma.

The Ritchey-Chretien design represents a successful attempt to further improve the image quality by using two hyperboloidal surfaces. The resultant image is now limited only by astigmatism and field curvature but involves the fabrication of two expensive aspheric surfaces.

Our fourth candidate, the Schmidt system, radically departs from the design of the first three candidate systems. It employs a relatively easily fabricated spherical primary and no secondary focussing element. This is shown in Figure 6a. It employs the powerful concentric principle. If the entrance aperture of the system is located at the center of curvature of the reflecting surface then the resulting image is free of coma and astigmatism. To correct the remaining spherical aberration the Schmidt design employs an aspheric corrector plate which is located at the center of curvature of the primary as shown also in Figure 6a. With this addition the image now suffers only from field curvature; that is, the image appears on a curved focal plane. Although the imagery from the Schmidt system is very good both on and off axis, the fabrication of the aspheric corrector plate greatly increases cost and so is not consistent with the requirement for achieving minimum tactical system cost in quantity.

The fifth candidate shown in Table 1 and in Figure 6b is the Maksutov system. This design also employs the concentric principle but

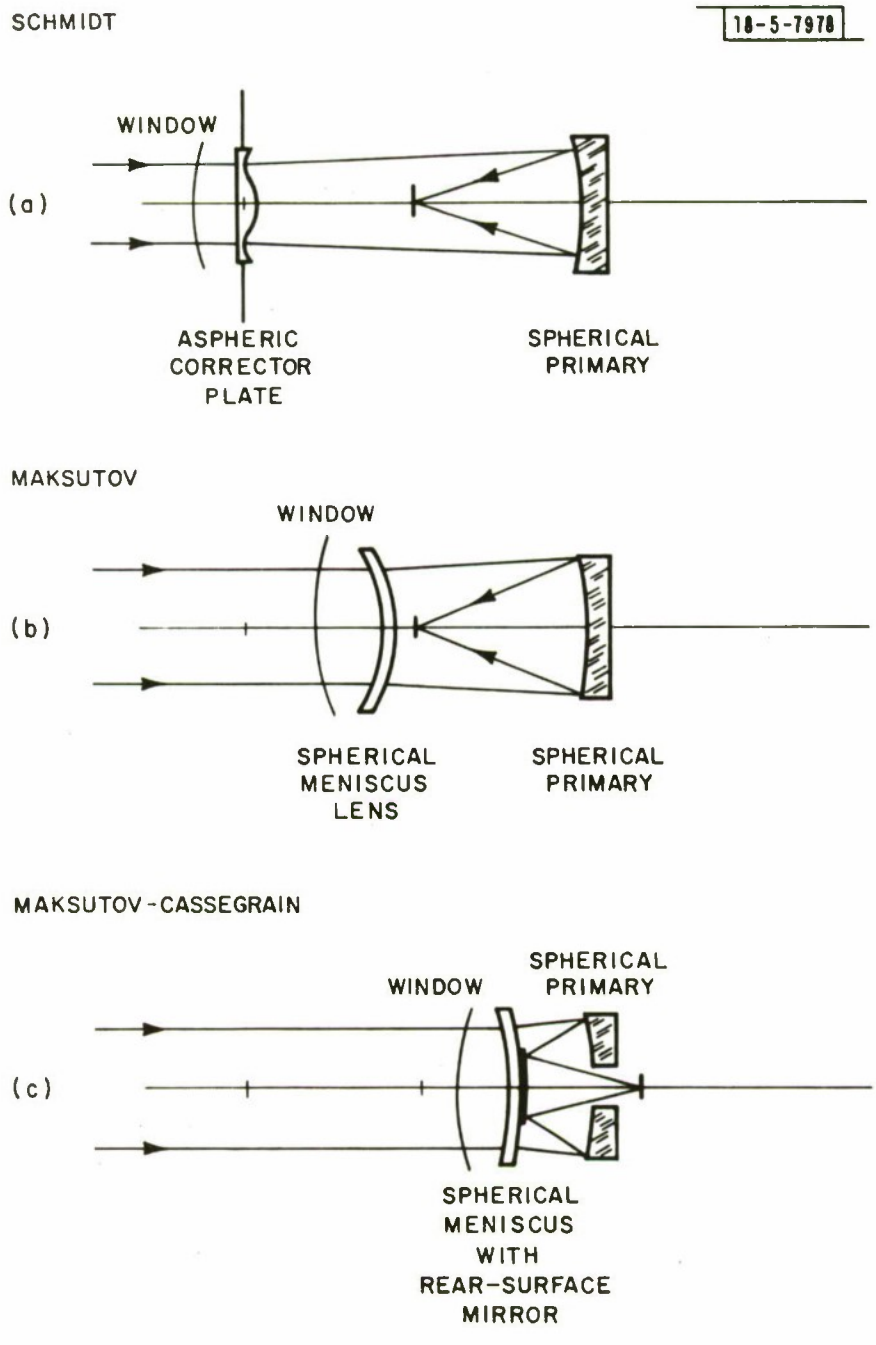

Fig. 6. Arrangement of surfaces in candidate telescope designs.

replaces the expensive aspheric Schmidt corrector plate with a relatively inexpensive spherical meniscus element. The correction of spherical aberration is not as good as in the Schmidt system.

Finally, we consider the Maksutov-Cassegrain design shown in Figure 6c. Comparison of the length of the configurations shown in Figure 6, which all have the same f/no., indicates the compactness of the Maksutov-Cassegrain system. In the arrangements shown, the rear surface of the meniscus element can support a mirror to direct the image to its focus behind the primary. The image surface is still curved but this can be corrected with a small refracting or reflecting element placed near the image.

Figure 7 shows the angular blur diameter which we have calculated for each of these configurations as a function of the off-axis angle. The maximum off-axis angle at which the blur diameter is acceptable is a measure of the FOV of the system. The solid lines represent calculations based on geometrical optics and a knowledge of the residual aberration for each system. The dashed line shows the diffraction limited blur diameter, $2\lambda/D$, for a 20 cm diameter aperture at $\lambda = 10\mu m$. When the solid line falls below the dashed line the system is essentially diffraction limited.

The excellent on-axis geometrical image quality obtained with the Dall-Kirkham, the Classical-Cassegrain, and the Ritchey-Chretien, all at f/3, can be seen. However, the first two are limited to small fields-of-view of less than 0.5^{o}. More compact systems of smaller f/no. would produce even worse results. At f/3 the Ritchey-Chretien has a field of

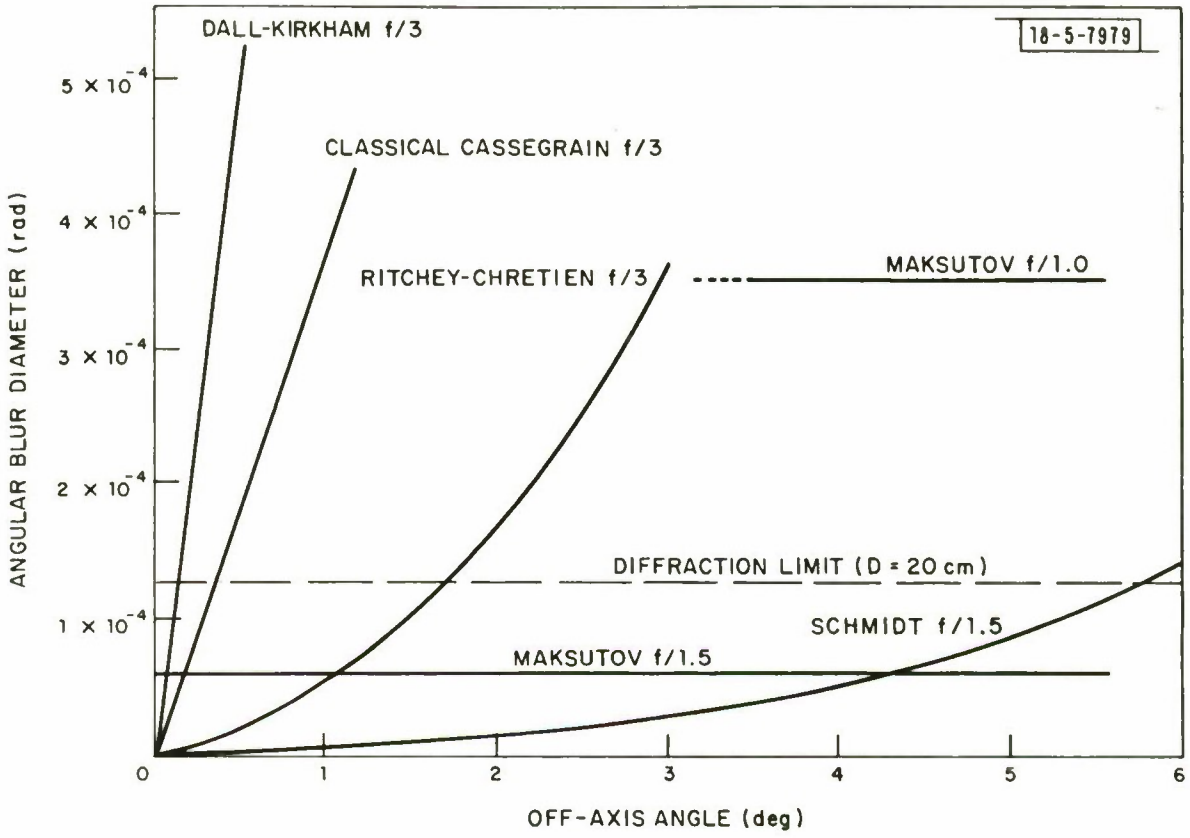

Fig. 7. Angular resolution vs. FOV for candidate optical systems.

1.5^{o}-2.0^{o}. However, as seen earlier, the fabrication of the required hyperboloidal secondary is expensive. The Schmidt performance is also excellent, even in a more compact f/1.5 design. The FOV is greater than 5^{o} in this case. Again, however, the aspheric element is expensive and we avoid this fabrication problem when possible.

The two horizontal solid lines in Figure 7 represent compact Maksutov or Maksutov-Cassegrain designs at f/1.0 and f/1.5. The lines are horizontal because the residual spherical aberration is independent of field position. Even though the f/1.5 system provides larger geometrical blur on axis than any of the other systems, it is essentially diffraction limited for the small aperture diameter and long infrared wavelength of interest in this application. The Maksutov-Cassegrain is therefore eminently suitable for use in the optical system of this tactical sensor. The resolution is essentially diffraction limited. The FOV is adequate for the high resolution identification mode as shown in Figure 4. The design can be made compact and lightweight. Finally, because it involves only spherical surfaces it can be manufactured in quantity at relatively low cost.

The smaller optical components of a sensor such as small lenses, mirrors, beam splitters, etc. are not examined here. These components, while important do not have a major impact on system capabilities or limitations and do not impact strongly on system size, weight, or cost.

IV. HETERODYNE ARRAY ANTENNA/RECEIVER

In previous sections we have determined the general system requirements

for a tactical sensor which will perform both search and identification. We have also considered the optical system designs which are suitable. At this point in the design study we turn our attention to the detection methods to be used.

As stated earlier, MTI provides an effective discriminant during search to separate targets from background. MTI search techniques require the use of coherent detection. There are also significant advantages in the use of coherent detection to increase SNR in the narrow field identification mode. The subject of this section is then the use of coherent heterodyne detection in a tactical laser radar.

Heterodyne detectors at infrared wavelengths exhibit antenna properties[5]. The reason for this is that the mixing mechanism at these short wavelengths is a spatial mixing of signal and local oscillator (LO) wavefronts at the surface of a photodetector. Heterodyne operation depends on constructive interference of these two wavefronts across the detector surface and this in turn requires that the angle of the received signal beam fall within λ/D of the angle defined by the LO. Heterodyne detection therefore exhibits the angular receiving characteristics which are usually associated with an antenna. These antenna characteristics play a primary role in determining the performance and the design requirements of an infrared heterodyne laser radar - particularly when the mission requires the use of detector arrays.

The necessity of using arrays was shown earlier. Figure 4 showed that an array of n detectors can reduce the azimuth search scan rate by a

factor n to bring it within the range of current scanner technology. Figure 5 showed that in the narrow field imaging mode the use of an array reduces the bandwidth to achieve adequate FOV and frame rate while maintaining optimum laser PRF.

The use of detector arrays in a heterodyne laser radar presents the designer with unusual requirements which are not present when using arrays in passive sensors. These unusual requirements are associated with the necessity for phase and amplitude matching of the local oscillator (LO) wavefront at the surface of each detector element. Consider the arrangement of n detectors in a linear array shown in Figure 8. The signal wavefront (S) which is incident on an individual detector is essentially a plane wave near the focus. The wavefront is incident on the detector from a direction which is found by drawing the ray from the center of the exit aperture to the individual detector. The signal amplitude distribution across the detector is essentially that of a diffraction limited aperture. To illustrate the unusual requirement we consider an LO wavefront which is a plane wave across the entire array. As shown in the insert there is then an angle ϕ between the signal and LO wavefronts. The LO amplitude across the detector is uniform.

It can be seen from Figure 8 that those detectors which are located at larger distances from the optical axis have increasingly larger angles between the signal and LO wavefronts. The antenna theorem[5], however, requires that

$$\phi < \frac{\lambda}{d} \tag{5}$$

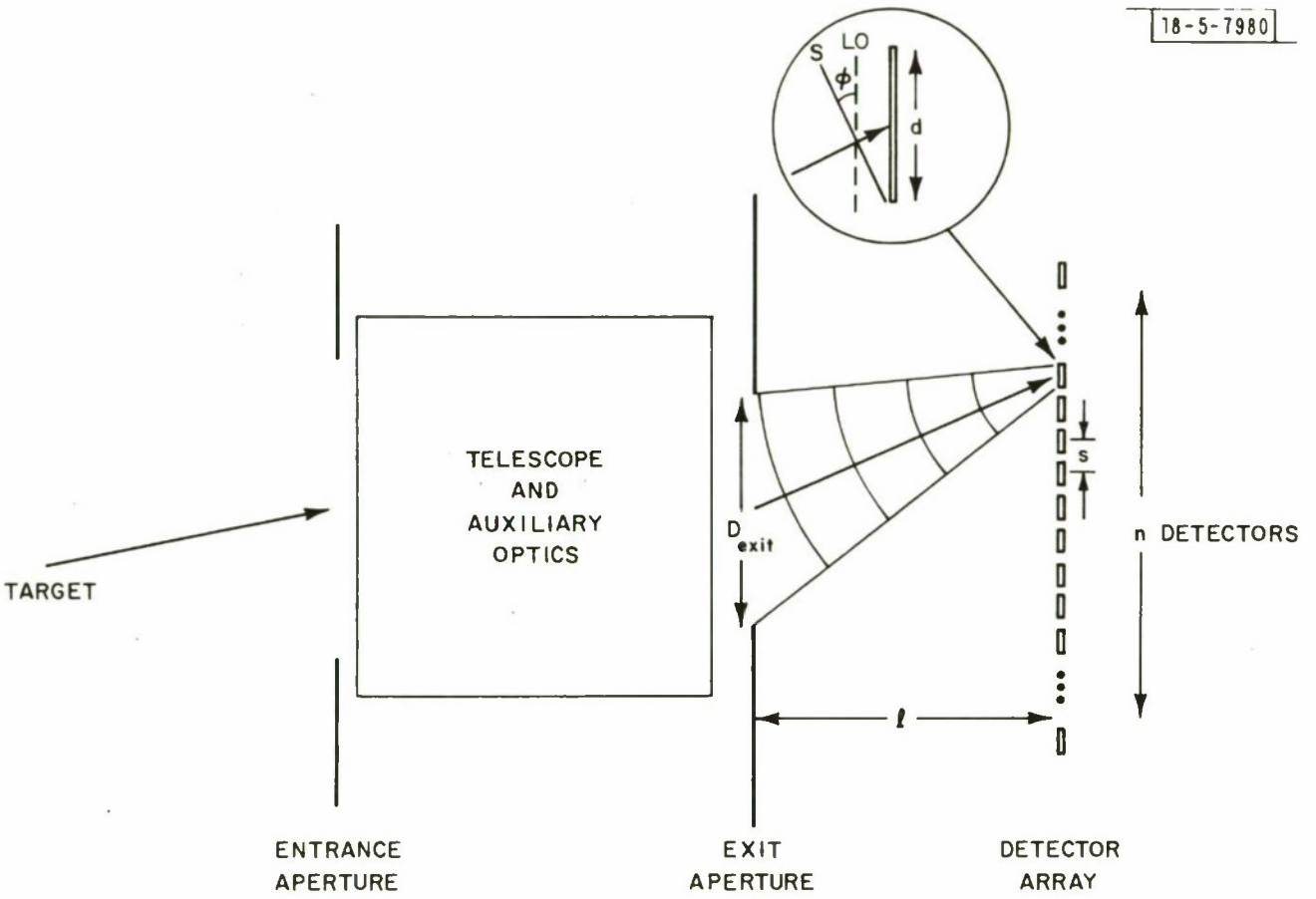

Fig. 8. Local oscillator phase and amplitude matching conditions for n element detector array.

to obtain heterodyne detection where ϕ is the angle between the signal and LO wavefronts, λ is the wavelength, and d is the diameter of the detector. The angle ϕ for the first detector off axis is found from the figure to be $\phi \sim s/\ell$ where s is the separation of detector centers and ℓ is the distance from exit aperture to image plane. For the outside detector then $\phi \sim ns/2\ell$. To meet the antenna theorem requirement $ns/2\ell < \lambda/d$ or

$$n < \frac{2\lambda\ell}{s\ d} \tag{6}$$

where

n = no. of detectors across linear dimension of array

λ = wavelength

ℓ = distance from exit aperture to image plane

s = center-to-center detector separation

d = detector linear dimension

The restriction implied by (6) severly limits the size of the detector arrays which can be used in a heterodyne receiver if a plane wave local oscillator beam is used. In addition, of course, the inner detectors even when adequately matched in phase are not matched in amplitude to the signal beam because the LO amplitude is uniform.

To overcome the heterodyne array size limitation described by (6) we now describe two new approaches to local oscillator wavefront control. The first provides phase matching and the second provides both amplitude and phase matching. With these techniques the advantages of using large detector

arrays in heterodyne receivers can be realized.

The first technique is the use of a cylindrical wave which emanates from the center of the exit aperture as shown in Figure 9a. The auxiliary optics required to focus the LO beam into the exit aperture are not shown. As the LO wavefront emanates from the exit aperture it creates an expanding cylindrical wavefront. As shown in the insert in Figure 5a this wavefront is parallel to the signal wavefront at each detector. This method then satisfies the requirements of LO phase matching. However, the amplitude is uniform and so is still not matched to the signal amplitude pattern at the detector.

A second concept of heterodyne array detection is shown in Figure 9b. The unique feature of this concept is the use of a holographic grating to create an array of n discrete local oscillator beams. The scale and positioning of the grating is arranged so that each plane wave leaving the grating is focussed by the last lens element onto the appropriate detector element just as the signal beam from the various parts of the target scene are focussed. This method has the advantage over the previous technique that it provides amplitude as well as phase matching.

The advantages of providing both amplitude and phase matching rather than just phase matching are as follows. First, the signal-to-noise ratio is increased. Analyses show[7,6] that for a system employing a partially obscured aperture such as the Maksutov-Cassegrain design shown in section III, there is a 3 dB improvement of SNR. The second advantage is that the angular resolution or image sharpness is improved[7]. There is approximately

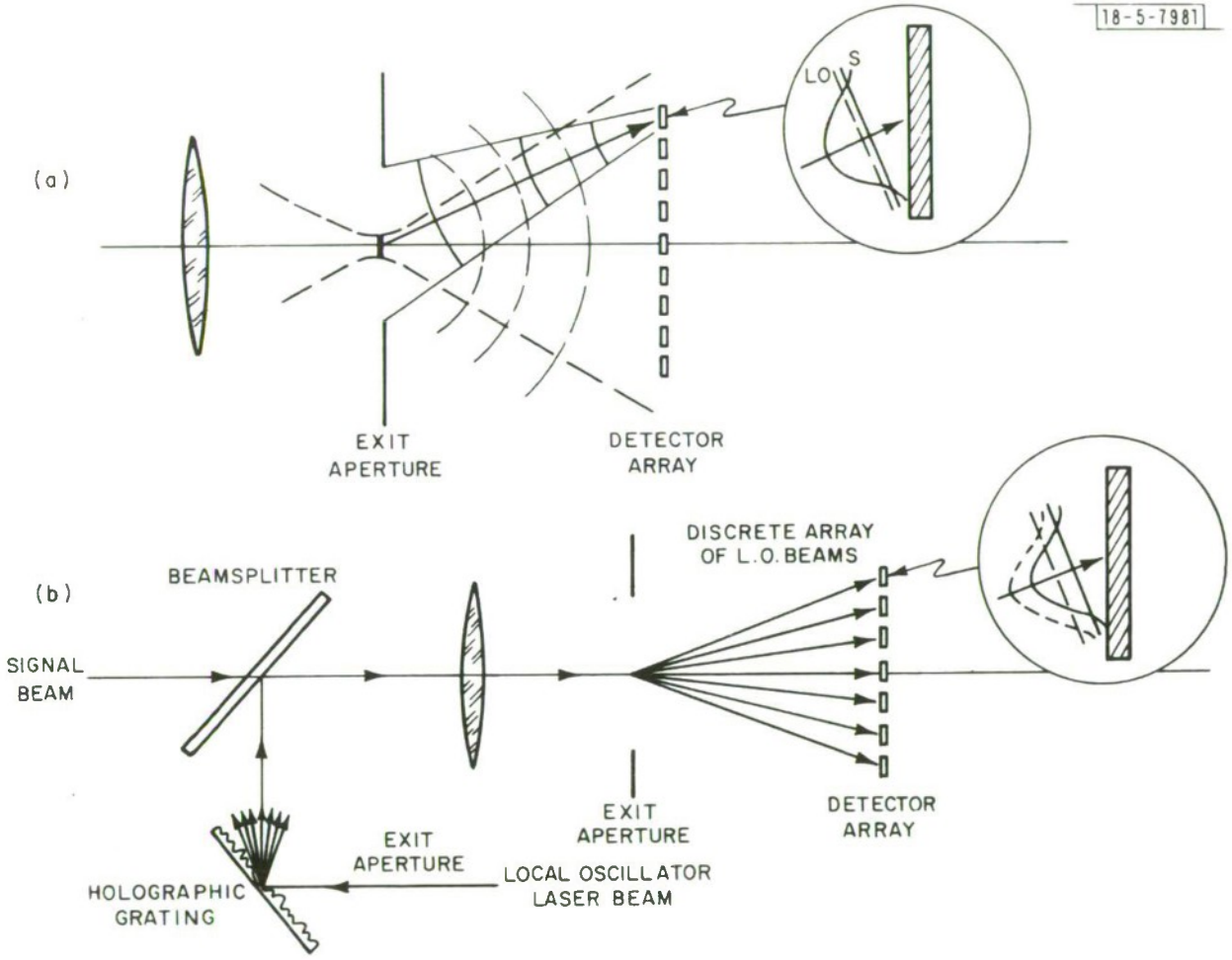

Fig. 9. Cylindrical wave and holographic grating heterodyne mixing concepts.

a 40% improvement in both the angular resolution and the modulation transfer function (MTF). Furthermore, when the local oscillator is matched in both amplitude and phase to the signal beam, the angular resolution is improved by a factor of 1.4 to 2.0 over the resolution of a passive sensor, depending on the form of the transmitter antenna pattern on the target.

Figure 10 shows a configuration for both amplitude and phase matched system operation. This arrangement integrates the design concepts of sections 3 and 4 for target recognition and identification at the required frame rates and over the required FOV. In the next section we consider target detection over a wide FOV using MTI techniques.

V. MTI DETECTION AND SIGNAL PROCESSING

As was pointed out in section 2a, wide field search and detection requires an effective discrimination technique to separate targets from background or "clutter". Moving target indication (MTI) has proven to be an effective discriminant at microwave frequencies. In this section we examine the detection capability of an infrared MTI search sensor using a CO_2 laser and heterodyne detection at 10.6μm.

A 10.6μm tactical airborne MTI radar offers two unique potential advantages over a microwave MTI radar in the air-to-ground application. These are (1) high signal processing gain, (2) low ground clutter. In combination they permit detection of moving ground targets with radial velocity less than 1 mph over 30° field of view with only a 20 cm forward looking aperture.

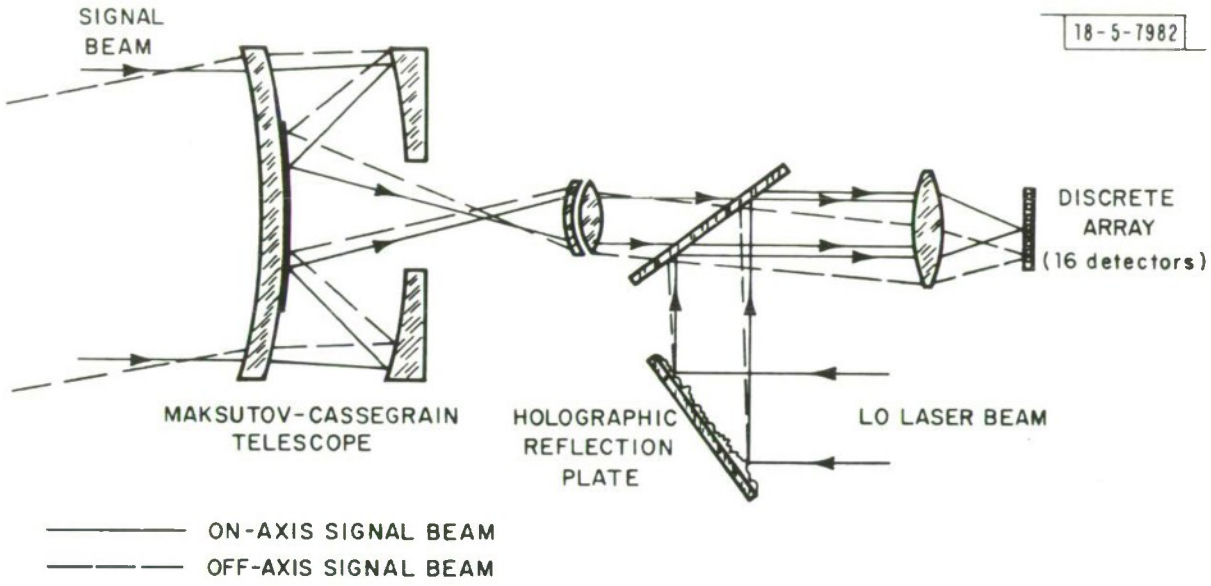

Fig. 10. Heterodyne array antenna/receiver.

The high signal processing gain is achieved by integration of returns from adjacent uncorrelated spatial resolution cells on the target. This gain is not available from microwave attack radars because the returns are correlated over the extent of the large beam width.

Low ground clutter is a consequence of the narrow beam width of the 10.6μm system. Microwave radars are usually limited by ground clutter. Frequency spreading due to ground clutter is reduced in the high resolution 10.6μm system to where it is roughly comparable to the doppler spread introduced by short term laser stability and by scan dwell time.

Signal Processing Gain

The scenario of interest involves a tactical attack aircraft at 200m altitude flying at Mach 0.5 in search of tanks and other targets. Terrain masking limits the range to less than 5 km and time considerations made it desirable to detect the targets at ranges greater than 3 km. At 10.6μm wavelength a 20 cm aperture provides a beam width of approximately 0.05 mr. At 4 km range this beam width subtends 20 cm on a target. The dimensions of a tank are approximately 6m length, 3m width, and 2m height. From the front or side the tank therefore subtends between 15 and 30 beam widths horizontally. As the scanning CW laser beam from the line scanner passes

across the tank the return signal can be sampled between 15 and 30 times to produce a series of uncorrelated but doppler shifted pulses. It is the integration or averaging of these pulses which produces the signal processing gain.

It is necessary to recognize that the target returns fluctuate in amplitude as the resolution cell scans across the tank. The statistics of pulse integration for fluctuating targets are known[8]. The particular statistics which apply here are known as Swerling 2. That is the probability density function for the received signal power is exponential so that

$$p(P) = \frac{1}{P_{av}} \exp\left[- \frac{P}{P_{av}} \right] \qquad P \geq o \qquad (7)$$

where P is the received signal power and P_{av} is the average. The returns from the adjacent spatial resolution elements are uncorrelated.

The procedure for determining the required signal to noise ratio per pulse, including the integration improvement factor, is as follows.

(1) Use Fig. 2.7 of Skolnik[8] to determine the required SNR in dB for a specified P_D and FAR for a single pulse and a nonfluctuating target.

(2) Use Fig. 2.23 of Skolnik to determine the additional required SNR in dB due to target power fluctuations as compared with a nonfluctuating target, again for a single pulse.

(3) Use Fig. 2.24 of Skolnik to determine the integration improvement factor to be realized by integrating n pulses.

For $P_D = 0.99$, FAR = 4×10^{-4}, Case 2 target statistics, and n = 15 to 30 this procedure gives the following results.

Initial SNR Requirement	15 dB
Pulse fluctuating target requirement	+17 dB
Minus pulse integration improvement	-26 to 28 dB
Net single pulse SNR requirement	5 dB

The signal processing gain realized through the integration improvement factor is approximately 27 dB.

Notice that in the microwave radar case which would correspond to Case 1 statistics where the pulses are correlated the comparable result would be

Initial SNR Requirement	15 dB
Plus fluctuating target requirement	+17 dB
Minus pulse integration improvement	-10 dB
Net single pulse SNR requirement	22 dB

By comparison, the high spatial resolution of the 10.6μm radar provides 17 dB additional signal processing gain which is not available with the wide beam width microwave system. Although this is not a complete assessment of the relative performance of microwave and infrared MTI radars, it does indicate the nature of the signal processing gain available at 10.6μm.

Minimum Target Velocity

Three factors determine the minimum radial target velocity which can be detected by a 10.6μm MTI radar. These factors and some typical values

for the associated frequency spread are

	Std. dev. of frequency
(1) laser frequency stability (short term)	$\sigma_\ell \sim 30$ KHz
(2) ground clutter (20 knots wind)	$\sigma_c \sim 42$ KHz
(3) scan dwell time (30° FOV at 2-5 km)	$\sigma_d \sim 17\text{-}106$ KHz

These values for the frequency spread σ are obtained as follows. The short term laser frequency stability is that which is not simply correctable by low frequency closed loop PZT tuning. The 30 KHz stability is available in an inexpensive commercial CO_2 laser. The ground clutter parameter is obtained from velocity data in the literature[9] using the relation

$$\Delta f = \frac{2}{\lambda} \Delta v \tag{8}$$

where Δf is the frequency shift, Δv is the velocity change, and λ is the wavelength. For wooded hills, the data in the literature shows that a 20 knot wind (10.2 m/sec) will cause a standard deviation in velocity of 0.22 m/sec for blowing vegetation within the beam. This value of Δv corresponds to $\Delta f = 42$ KHz.

Scan dwell time varies with range. The relation between the system parameters and the frequency spread Δf due to finite line scanner dwell time is

$$\Delta f = \frac{vh\ (FOV)}{n\ \theta^2\ R^2} \tag{9}$$

where

v = aircraft velocity = 165 m/sec

h = aircraft altitude = 200m

FOV = full field of view = 30^{o} or 60^{o}

n = number of detectors = 16

θ = angular resolution = 0.05 mr

R = range to target = 2-5 km

An evaluation of the scan dwell time for these parameters leads to the 17-106 KHz standard deviation indicated above. The lower frequency spread corresponds to the longer range.

Since the three frequency spreading mechanisms are uncorrelated we take the total frequency variance to be

$$\sigma^2 = \sigma_{\ell}^2 + \sigma_c^2 + \sigma_d^2 \qquad (10)$$

To evaluate the minimum MTI target velocity which can be detected we must specify the signal processing further. The MTI system block diagram is shown in Figure 11. A tunable electronic local oscillator uses the available information on scan angle of the optics and relative velocity between aircraft and ground to shift the incoming IF signal to a low frequency. A notch filter eliminates the low frequencies corresponding to no moving target and passes any target energy which is doppler shifted to higher or lower frequencies. A rectangular filter function as shown in the diagram is certainly not optimum. It is used here only for calculating convenience.

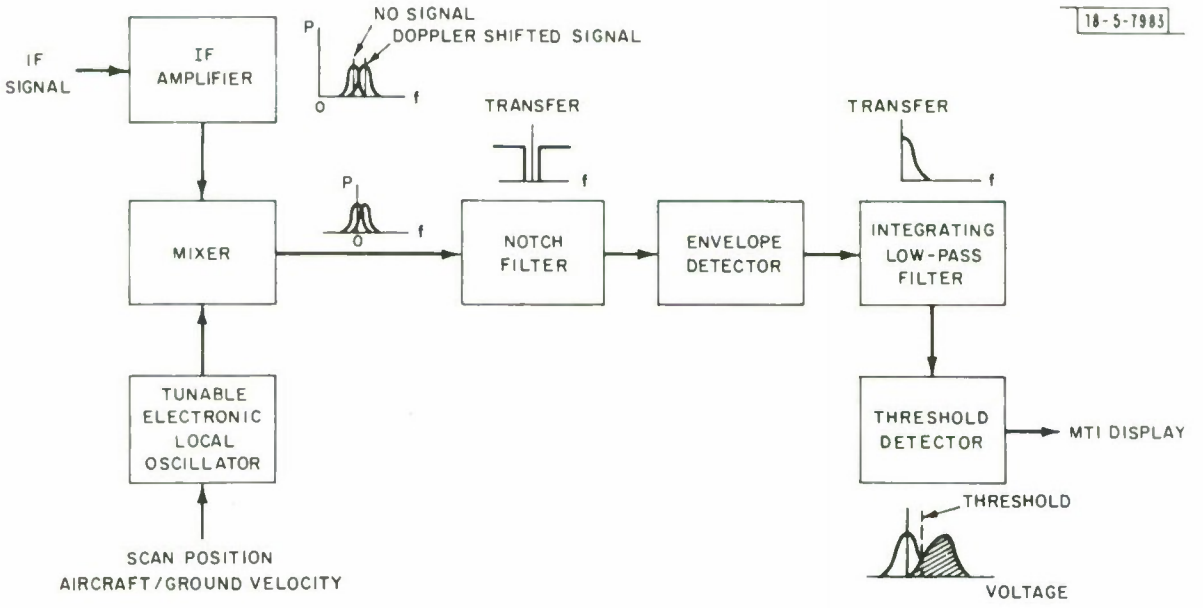

Fig. 11. MTI signal processing block diagram.

The optimum filter is the matched filter given by

$$T(f) = k \frac{S^*(f)}{|N(f)|^2} \tag{11}$$

where

$T(f)$ = transfer function

f = frequency

$S(f)$ = signal spectrum

$N(f)$ = noise spectrum

k = constant

Measurements and calculations can show the optimum $T(f)$.

The notch filter is followed by an envelope detector and then by the integrating low pass filter which has a cutoff frequency adequate for integration of 15 to 30 independent samples of the return from the target. Obviously the signal need not actually be sampled. The integration may be completely analog. The integrator output is passed to a threshold detector which indicates the presence of a moving target when the threshold is exceeded.

The previously calculated 5 dB required SNR per pulse means that the signal must be 3.2 times larger than the noise at the output of the notch filter. When the noise spectrum and the signal spectrum (doppler shifted noise spectrum) are gaussian this will be achieved when the cutoff of the notch filter (effectively the MTI frequency threshold) is set equal to σ, the total standard deviation of frequency spreading due to laser

instability, ground clutter, and dwell time. Using the previous specified data from total frequency spread the effective velocity threshold is found to be less than 1 mph at 4 km as shown in Figure 12.

This figure also shows the minimum target velocity detectable by an existing K_u band radar on the F-111 aircraft for comparison. The microwave radar is limited by internal motion ground clutter. The IRAR 10.6μm system is limited by dwell time at short ranges and by both laser stability and ground clutter at longer ranges. Some forward looking microwave radar systems now in the design stage are also expected to provide radial velocity thresholds of approximately 1 mph.

The preceding design analysis indicates that a 10.6μm MTI radar can provide the discrimination required for wide field search and detection of tactical targets.

VI. IMAGE SIGNAL-TO-NOISE RATIO

Figure 13 shows a diagram of an infrared heterodyne laser radar system which produces a displayed image. Some of the essential operating components such as scanners or feedback control loops are omitted from simplicity. The portions of the system which are shown are those which most directly determine the signal-to-noise ratio (SNR) of the image. Some characteristics of the human visual system must also be considered in determining SNR.

We have said earlier that in the narrow field imaging mode it is advantageous to use a pulsed laser transmitter in order to provide data on

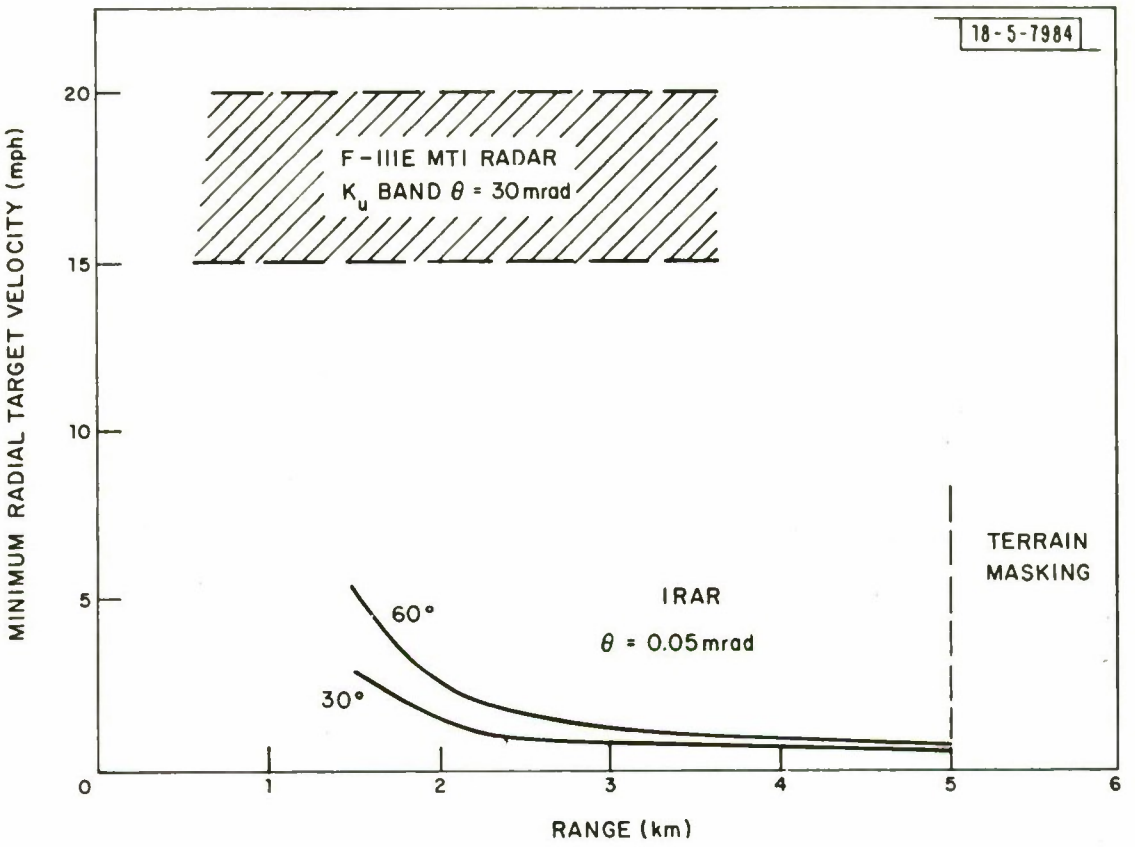

Fig. 12. MTI target search: minimum radial target velocity vs. range.

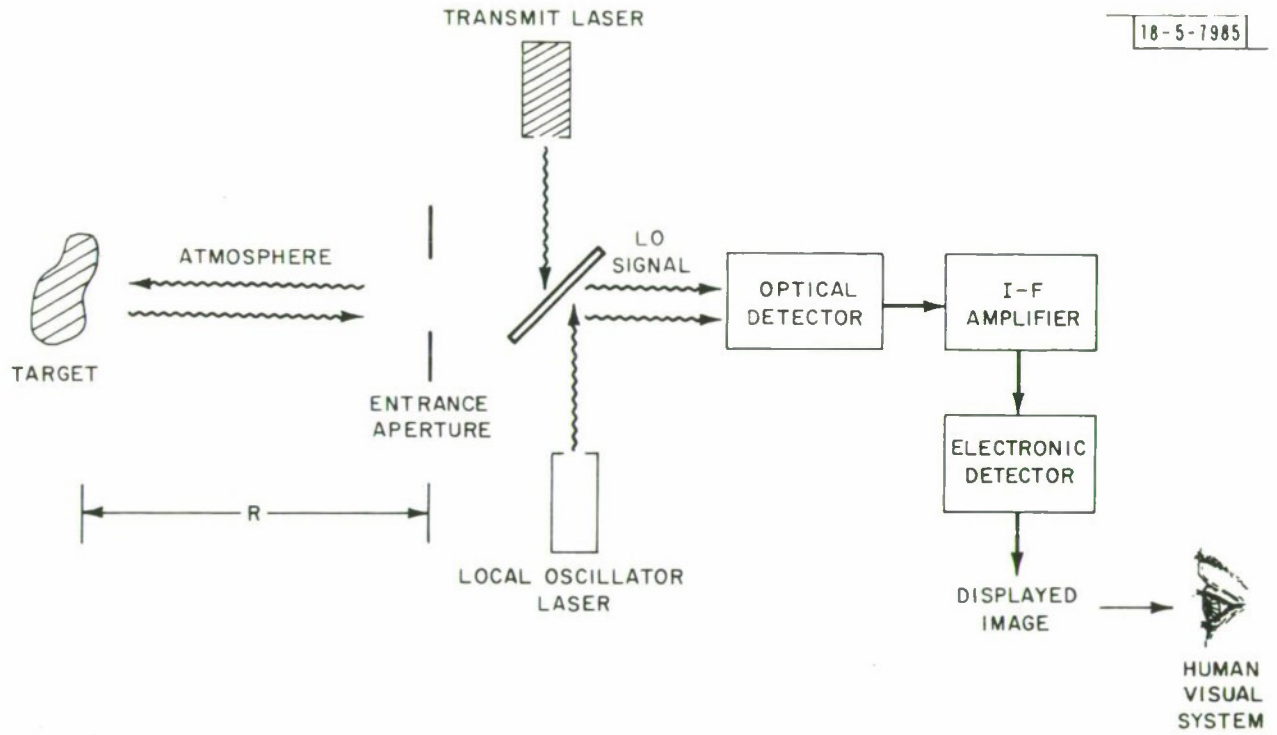

Fig. 13. Infrared heterodyne laser radar system diagram showing components involved in determining image SNR.

range R to the target. The following assumes that the bandwidth B of the I-F amplifier shown in Figure 13 is matched to this pulse width so that $B \sim 1/t_p$ where t_p is the transmit laser pulse width. In this situation the following analysis will be found to apply equally to either pulsed or CW transmit lasers.

In an optical heterodyne receiver the signal-to-noise ratio is limited by the photon shot noise associated with the local oscillator laser beam[10,11]. The electrical power SNR, designated SNR_p, at the image display is approximately

$$SNR_p = \frac{P_R}{h\nu\ B} \tag{12}$$

when the electronic detector is a linear envelope detector and where

P_R = effective received average signal power at the image display

$h\nu$ = L.O. photon energy

B = I-F bandwidth

Notice that (12) is equivalent to $SNR_p = E_R/h\nu$ where $E_R = P_R/B$ is the received signal energy per transmitted pulse. The SNR_p is then equal to the number of received photons in each pulse.

The effective received power is related to the parameters of the other system components shown in Figure 13 in the following way. The fraction of the transmitted optical power P which reaches the target is $P\ e^{-\alpha R}$ where R is the range and α is the atmospheric attenuation coefficient.

The reflected power is then $P \rho e^{-\alpha R}$ for a target of directional reflectance ρ. If the target is optically rough so that this power is scattered over a hemisphere (see section 8) then the radiant intensity or power per unit solid angle which is reflected from the target is $P \rho e^{-\alpha R}/\pi$ where π is the effective solid angle. The power collected by the entrance aperture on passage back through the atmosphere is then $P \rho e^{-2\alpha R} A/\pi R^2$ where A is the aperture area. Taking into account the quantum efficiency η of the optical detector and the combined internal optical and electrical efficiency of the system the effective received signal power at the image display can be written

$$P_R = \frac{P \rho e^{-2\alpha R} A \varepsilon \eta}{\pi R^2} \tag{13}$$

so that the electrical power SNR at the image display is

$$SNR_p = \frac{P \rho e^{-2\alpha R} A \varepsilon \eta}{h\nu B \cdot \pi R^2} \tag{14}$$

where

- P = laser transmitter average power
- ρ = directional reflectance of rough surface target (see section 8)
- α = atmospheric attenuation coefficient
- R = range from entrance aperture to target
- A = entrance aperture area
- ε = optical and electronic efficiency factor

$h\nu$ = local oscillator photon energy

B = I-F amplifier bandwidth

Equation (14) is the basis for evaluation of system performance under varying weather conditions in section 8.

In order to provide a basis for comparing the image SNR of an infrared laser radar with that of a passive forward looking infrared (FLIR) system we now consider the FLIR SNR. It may be said with some justification that a comparison of an infrared airborne radar (IRAR) with a FLIR is a comparison of apples and oranges. The FLIR utilizes the thermal emission contrast between targets and backgrounds to form images while the radar employs reflectivity contrast. The radar provides range data while the FLIR does not. Also, the electronic system components are in fact different because of the quite different detection methods used - direct detection in the case of the FLIR and heterodyne/conversion followed by envelope detection in the case of IRAR. Nevertheless a comparison is necessary to gain some understanding of relative performance since both systems produce a displayed image.

For a FLIR the voltage SNR at the image display[12] is

$$SNR_V = \frac{P_R}{NEP} \tag{15}$$

where the optical power to voltage relation is due to the square law conversion inherent in direct detection and where NEP, the noise equivalent power, is given by NEP = $\sqrt{a\,B}\,/D^*$ with a being the detector surface area, B the bandwidth, and D* the specific detectivity of the detector. To

determine P_R we consider the collection of radiant power by the FLIR.

The power per unit area emitted by a hot target is M, the radiant exitance. The radiant exitance different between a target and its background is then $(\partial M/\partial T)\ \Delta T$ where ΔT is the effective temperature difference. The radiance then becomes $(\partial M/\partial T)\ \Delta T/\pi$. To determine the radiance at the FLIR entrance aperture we multiply this by the atmospheric transmittance $e^{-\alpha R}$. The radiant power at the entrance aperture can then be written $A\theta^2\ (\partial M/\partial T)\ \Delta T/\pi$ where A and θ are the area of the entrance aperture and the instantaneous field of view (IFOV) or angular resolution of the FLIR. Taking into consideration the overall optical and electrical efficiency of the system the voltage SNR at the image display is

$$SNR_V = \frac{A\theta^2\ \varepsilon\ e^{-\alpha R}\ \left(\frac{\partial M}{\partial T}\right)\ \Delta T}{\pi \cdot NEP} \qquad (16)$$

which is related to the power SNR approximately by $SNR_p = (SNR_V)^2$ and where

A = entrance aperture area

θ = IFOV of FLIR

ε = optical and electrical efficiency

α = atmospheric attenuation coefficient

R = range from entrance aperture to target

ΔT = effective temperature difference between target and background including emissivity effects

NEP = noise equivalent power = $\sqrt{a\ B}\ /D^*$

Notice that for both the IRAR and the FLIR the SNR_p involves the bandwidth B. This bandwidth is given by equation (4) for a single detector. When an array of n detectors is used then the bandwidth becomes

$$B = \frac{\dot{F}\,(FOV)^2}{n\,\theta^2} \tag{17}$$

where $\dot{F}$ is the frame rate, FOV the scan field of view, and θ the angular resolution.

With either the IRAR or FLIR system there is some improvement of SNR_p due to the temporal integration properties of the human visual system. The visual system has a characteristic response time between 0.1 and 0.2 second. An image presented at 30 frames per second therefore involves some frame integration. Since the integration corresponds to an incoherent summation the improvement in voltage SNR at the display is proportional to $\sqrt{N}$ where N is the number of frames integrated. This means that the improvement in SNR_p is proportional to N.

The other signal processing property of the visual system which should be taken into account is its angular integration property. If the angular resolution element of the visual system subtends more than one displayed image element then there is a further increase in SNR_p but with a concomitant loss of image spatial detail. This spatial integration can be important when the image is speckled as described in the next section.

Equations (14) and (16) will be used in section 8 to show the superior performance of an infrared heterodyne radar over a FLIR of comparable size, weight, and cost in the bad weather which is typical of Central Europe.

VII. IMAGE PROCESSING

There are two signal or image processing issues which must be addressed in a design study for an infrared airborne radar. The two issues are image speckle and glints. Both are associated with the surface reflecting characteristics of targets and backgrounds.

Image speckle[13] is the random grainy appearance of images which have been formed with lasers. It occurs when the temporal coherence length of the laser is longer than the optical depth of the target within the beam. The phenomenon occurs with CO_2 lasers which have coherence lengths which are typically many meters, but may not occur with other lasers such as Nd:YAG which have short coherence lengths. The envelope of the complex field amplitude at the receiver is known to have a Rayleigh probability density function while the optical power at the receiver is exponentially distributed. The autocorrelation function of the speckle pattern in the image extends over approximately two resolution elements corresponding to the angle $2\lambda/D$ in object space.

One technique for reducing the effects of image speckle is frame averaging or summation. The summation of n uncorrelated speckled images reduces the standard deviation of power in proportion to $\sqrt{n}$. The requirements for obtaining uncorrelated images can be found as follows.

Consider the geometry of a low altitude high velocity tactical aircraft as shown in Figure 14. The power pattern produced on the ground at range R by a transmit beam of aperture D has a linear dimension in the forward direction which is given approximately by $L = \theta R/\cos\beta = \lambda R/D \cos\beta$.

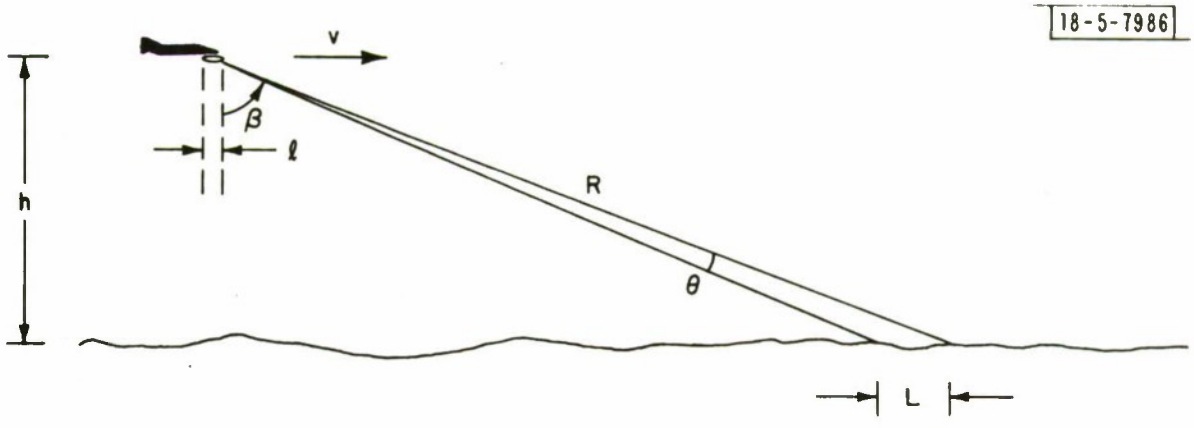

Fig. 14. Geometry for determining image decorrelation distance of infrared airborne radar.

From the theory of the propagation of partially coherent beams of radiant power it is known that the power pattern on the ground with this linear dimension will produce a field in space which is correlated over a linear distance given by $\lambda R/L$ or, by using the relation for L found above, by D $\cos\beta$. But the distance D $\cos\beta$ is just the projected length of the aperture along the forward direction. The minimum time between image frames which will insure that the images are uncorrelated is then $t = D \cos\beta/v$. The maximum frame rate at which uncorrelated images can be obtained is therefore

$$\dot{F}_{max} = \frac{v}{D \cos\beta} = \frac{vR}{Dh} \tag{18}$$

where

v = aircraft velocity

R = slant range to target

D = radar aperture diameter

h = aircraft altitude

Figure 15 shows the maximum frame rate which can be utilized as a function of slant range and aircraft altitude. Typical values of aircraft velocity and aperture diameter are taken to be v = 350 m/s and D = 20 cm. Notice that the minimum value of $\dot{F}_{max}$ occurs when h = R, where $\dot{F}_{max} = v/D$ that is when the sensor is looking straight down. At all other angles the maximum allowable frame rate is greater than v/D. For typical realistic values of aircraft velocity and sensor aperture diameter the image frames are always uncorrelated.

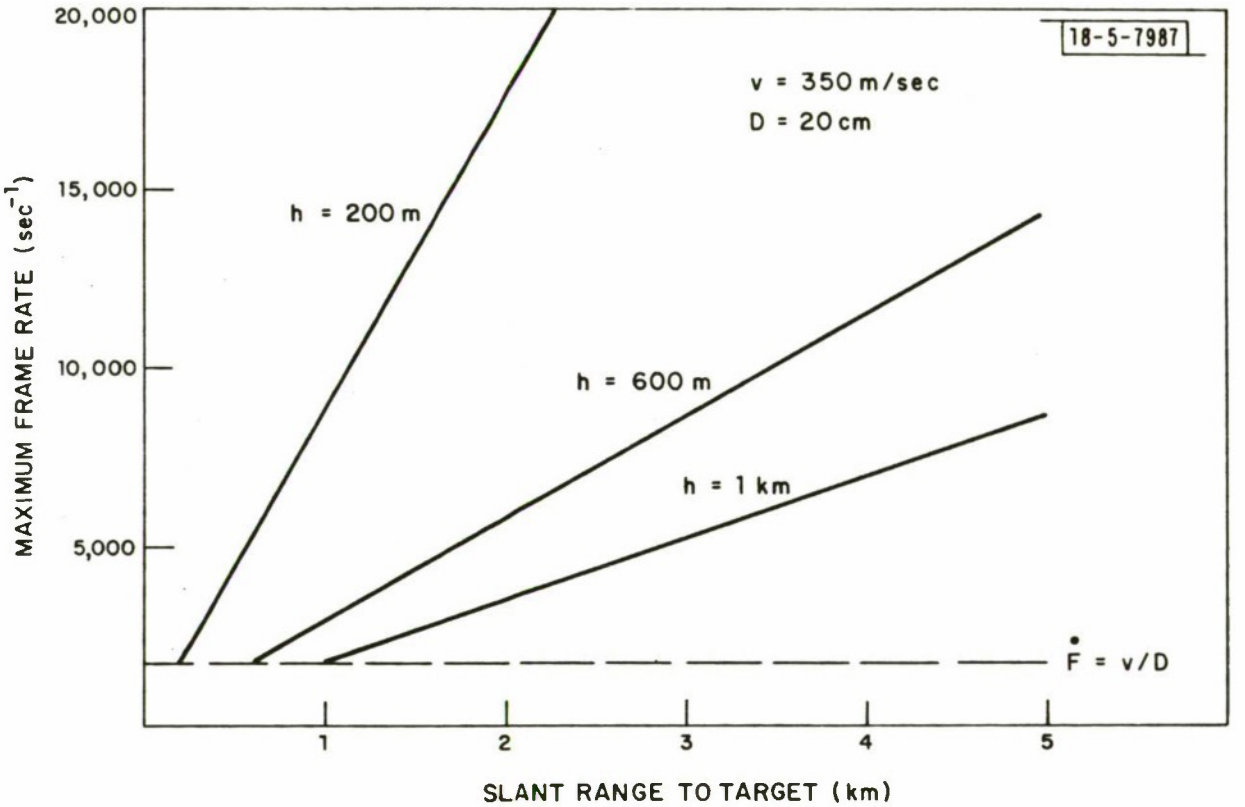

Fig. 15. Maximum frame rate to obtain uncorrelated image for image processing.

The second signal processing issue is glints. These are portions of the target surface where the geometry of the transmit beam and target surface orientation provide a very large signal return. Figure 16 shows the measured[14] bidirectional reflectance at $\lambda = 10.6\mu m$ of olive drab painted steel, typical of tactical targets. The curve shows a strong peak in the specular direction where the angle of incidence and reflection are equal. This is the property of targets which produces glints.

There are two questions associated with a target reflectance curve of the type shown in Figure 16. First, what type of signal processing is required and second, what are the limitations on this signal processing?

We can see from the figure that for changes in target surface orientation of 10 or 20^{o} the bidirectional reflectance may change by two or three orders of magnitude. Bidirectional reflectance is defined as

$$\rho' (\lambda; \theta_i, \phi_i; \theta_r, \phi_r) = \frac{L^r (\theta_r,\phi_r)}{E^i (\theta_i,\phi_i)} \tag{19}$$

where

θ_r,ϕ_r = polar angles of reflected power

θ_i,ϕ_i = polar angles of incident power

L^r = reflected radiance

E^i = incident irradiance

λ = wavelength

and where it is understood that the incident beam is linearly polarized in a specific direction and the receiver is linearly polarized in a specific

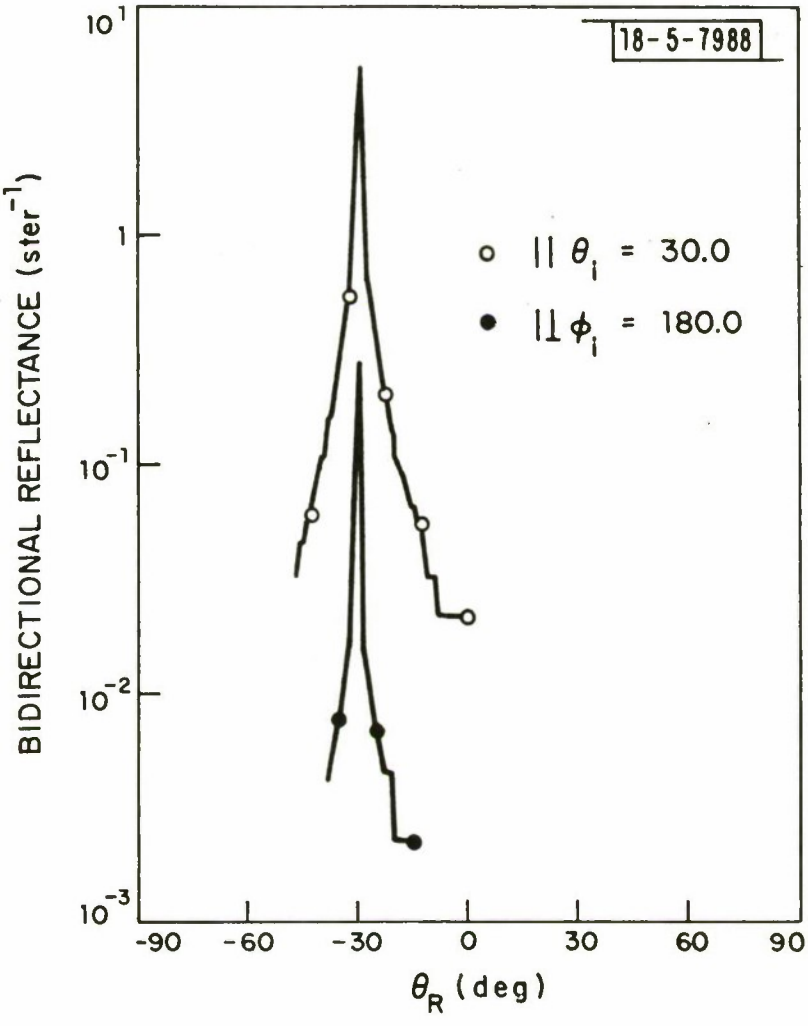

Fig. 16. Bidirectional reflectance of olive drab painted steel. $\|$ indicates parallel linearly polarized incident and received beams. $\|_{\perp}$ indicates crossed polarizations. The angle of incidence is 30^{o}. λ = 10.6μm (from reference 14).

direction, not necessarily the same. Since ρ' is proportional to the ratio of optical power quantities the optical power can change by orders of magnitude. The form of signal processing required is then some form of signal compression to enable the wide dynamic range of target reflectance values to produce a displayed image which covers a much smaller dynamic range. The displayed image dynamic range is limited by the display device itself and also by the input dynamic range of the human visual system. The signal compression is a point-by-point nonlinear transformation.

Although it is not possible to define this transformation without further study, it is possible to define its limitations in producing high quality images. The limitation occurs when the angular orientation of the target surface with respect to the incident beam is such that the bi-directional reflectance value produces a signal at the receiver aperture which is below the required minimum. Since the SNR_p at the receiver is specified by equation (14) in terms of the directional reflectance ρ of a diffuse target rather than the bidirectional reflectance ρ' it is necessary to establish the connection between them.

Since this relationship between ρ and ρ' is fixed only when the target is a diffuse reflector, we are actually establishing the bidirectional reflectance of an equivalent diffuse target which would produce the same SNR_p as the real target. By locating this value of bidirectional reflectance on the curve shown in Figure 16 it is then possible to find the angular range within which the target orientation will produce an SNR_p

which is just equal to the minimum requirement on ρ established through equation (14). This procedure permits an estimate of the angular limits of target orientation within which it is possible to produce useable imagery.

For a linearly polarized incident beam and a linearly polarized aligned receiver the relationship is $\rho' = \rho/\pi$ for a diffuse target. A typical value for ρ which is used for system evaluation in section 8 is $\rho = 0.05$. The corresponding bidirectional reflectance is $\rho' = 0.05/\pi = 1.6 \times 10^{-2}$ ster^{-1}. This value is below the lower limit of experimental data shown in Figure 16. However, it can be seen from the figure that this corresponds to angles of approximately $\pm$ 30^{o} from the angle of incidence. However, further interpretation and data are needed in this area. The geometry which led to the data of Figure 16 keeps the incident beam at 30^{o} from normal and varies the receiver angle. The radar geometry, however, keeps the transmit and receive directions parallel and changes the angle of both with the target surface.

The principal implication of the preceding is that signal compression methods are required. These methods are limited to the target angular orientations which correspond to the minimum SNR_p to produce adequate images.

VIII. SYSTEM PERFORMANCE UNDER VARYING WEATHER CONDITIONS

Weather is an important factor in the performance of tactical optical and infrared sensors. In this section we determine the expected weather

performance of the infrared airborne radar (IRAR) using a CO_2 laser transmitter and heterodyne detection. To establish a basis for comparison we determine the expected performance of a state-of-the-art FLIR under the same weather conditions. To further examine the active vs. passive sensor question we also define an advanced design FLIR which would utilize CCD/CID focal plane technology in an array of 10^4 detector elements. The weather performance of this advanced design is also compared with that of the IRAR system.

The basis for evaluation of the IRAR system is the image SNR relation derived in equation 14. FLIR performance is determined from equation 16. In both cases the weather parameters are based on a recent statistical analysis[15] of real weather data from a variety of locations in central Europe.

Performance of these systems under varying weather conditions can be described in terms of "operational utility". Operational utility is the fraction of the time for which the sensor system will provide adequate SNR_p at a specified range from sensor to target. A one-to-one correspondence can be established between a given level of atmospheric attenuation and the maximum range at which the sensor will provide adequate SNR_p. If the fraction of the time for which this attenuation occurs is known from weather data then the operational utility can be established. In the following we evaluate these sensor's for winter weather in central Europe. This weather represents an important test of expected system performance.

Table 2 shows attenuation values in dB/km extracted from a recent

TABLE 2

WEATHER AVERAGES/GERMANY (BERLIN, DRESDEN, ESSEN, HAMBURG)

dB/km	Frequency				1 - Frequency				1 - Frequency		
	No Rain		Rain		No Rain		Rain				
	S	W	S	W	S	W	S	W	Summer	Winter	
0	1.0	1.0	1.0	1.0	0	0	0	0	0	0	
0.5	.99	1.0			.01	0	0	0	.01	0	
0.75	.98	0.8			.02	.20	0	0	.02	.14	
1.0	.95	0.5	1.0	.99	.05	.50	0	.01	.04	.35	
1.25	.75	.37	1.0	.99	.25	.63	0	.01	.19	.44	
1.5	.53	.28	1.0	.99	.47	.72	0	.01	.36	.51	
1.75	.33	.24	1.0	.99	.67	.76	0	.01	.52	.54	summer.
2.0	.13	.20	1.0	.98	.87	.80	0	.02	.67	.57	winter ∿ equal
2.5	.07	.15	.95	.92	.93	.85	.05	.08	.68	.62	@1.8dB/km
3.0	.03	.11	.91	.82	.97	.89	.09	.18	.77	.68	
3.5			.67	.61			.33	.39	.83	.725	
4.0	.02	.09	.41	.56	.98	.91	.59	.44	.89	.77	
4.5									.905	.795	
5.0	.007	.07	.30	.46	.99	.93	.70	.55	.92	.82	
5.5									.935	.835	
6.0	.005	.06	.18	.36	.99	.94	.82	.63	.95	.85	

S = Summer W = Winter

analysis of real weather data based on the RAND weather data tapes. The first column represents a range of attenuation values. The second and third columns show calculated values for the frequency of occurrence of attenuation values which are greater than or equal to the value indicated. These represent an average of data from Berlin, Dresden, Essen, and Hamburg. Both summer and winter data are shown although only winter data will be used. The reference indicated does not include rain. It is therefore necessary to determine modified values for frequency of occurrence which include rain conditions. Columns four and five show the corresponding frequencies of occurrence in rain only based on a separate analysis of attenuation in rain. Columns 6-9 show the probability that the attenuation is less than or equal to the indicated attenuation.

In order to combine the probabilities representing rain and no rain it is necessary to know the relative frequency of occurrence of the two weather conditions. This is found from Figure 6 of the indicated reference.[15] The resultant values of probability of occurrence shown in columns 10 and 11 are then

$$(I\text{-}F) = (I\text{-}F)_{NR}\, P_{NR} + (I\text{-}F)_{R}\, P_{R} \tag{20}$$

where P_R is the probability of rain and P_{NR} is the probability of no rain. Clearly, $P_R + P_{NR} = 1$.

On the basis of these data we determine the range at which the IRAR system yields $SNR_p = 64$ or 18 dB. To specify the attenuation we use the

relation α = (dB/km)/4.3. Other parameters used in determining IRAR weather performance are shown in Table 3. These parameters have been selected to represent realistic component technology and also to be as close as possible to the corresponding parameters of the state-of-the-art FLIR to permit a realistic performance comparison.

Notice that the aperture diameter and frame rates of the IRAR and state-of-the-art FLIR are the same indicating comparable system size and weight. However, the IRAR system does utilize transmit and LO lasers while the FLIR utilizes a larger detector array. Also, the angular resolution of the FLIR is not as good as that of the IRAR system but the FOV is larger.

In order to provide further comparison of active and passive sensors column 3 of Table 3 shows the parameters at an advanced FLIR design which has the same high angular resolution and the same FOV as IRAR. We assume here that focal plane technology can progress to the point of providing a CCD/CID array of 10^4 elements with no direct penalty in D*. The loss of cold shielding in an array of this size is indicated by the change in cold shielding efficiency rather than by incorporating this factor into the D* value.

The FLIR performance calculations are based on the same weather statistics shown in Table 2. Equation (16) and the relation $SNR_p = (SNR_V)^2$ are used to determine the range at which a given attenuation leads to SNR_p = 64 or 18 dB. This requirement corresponds to SNR_V = 8 which is adequate to produce good imagery. None of the evaluations performed here

TABLE 3

SYSTEM PARAMETERS

Parameter		IRAR	State of the art FLIR	Advanced FLIR Design
Aperture Diameter		20 cm	20	20
Angular Resolution		0.05 mr	0.10 mr	0.05 mr
Field of View		9 mr	4^{o}	9 mr
Frame Rate		30	30	30
Laser Power		50 W		
Number of Detectors		16	180	10^{4}
Detectivity D*			4.10^{10}	4.10^{10}
Detector Radius			25μm	25μm
Target Signature ΔT			2.5 K	2.5 K
	Δρ	0.05		
Efficiencies	Optical	0.32	0.60	0.30
	Scan	0.75	0.75	0.75
	Quantum	0.70		
	Cold Shield		1.00	0.18

take into account the small improvement in signal-to-noise which arises from the temporal integrating characteristics of the human visual system. The change in performance is not significant when compared with the differences between the three systems involved.

Figure 17 shows the expected operational utility, or fraction of time operating, for the three sensors as a function of slant range from sensor to target. Ranges beyond 5 km are not considered because of terrain masking limitations. As indicated by the figure the IRAR system performance is significantly better than that of either FLIR system.

To indicate the difference in performance, Figure 17 shows two lines. The vertical line indicates that at a range of 2.5 km when the state-of-the-art FLIR can be expected to operate in 50% of all weather situations, the IRAR can be expected to operate in 80% of all weather situations. The IRAR system can therefore be expected to be much closer to an all-weather sensor system than the state-of-the-art FLIR. The horizontal line, on the other hand, shows that in a given weather situation when the state-of-the-art FLIR operates at ranges out to 1.5 km the IRAR system can be expected to operate out to ranges of 4.5 km. This factor of three advantage in operating range is large and is typical of the relative operating ranges of the two systems over a variety of weather conditions.

As shown in the figure, the advanced FLIR design does provide some improvement over the state-of-the-art FLIR due to the use of larger arrays of detectors. However, this is partially offset by the noise increase due to cold shielding problems with large arrays.

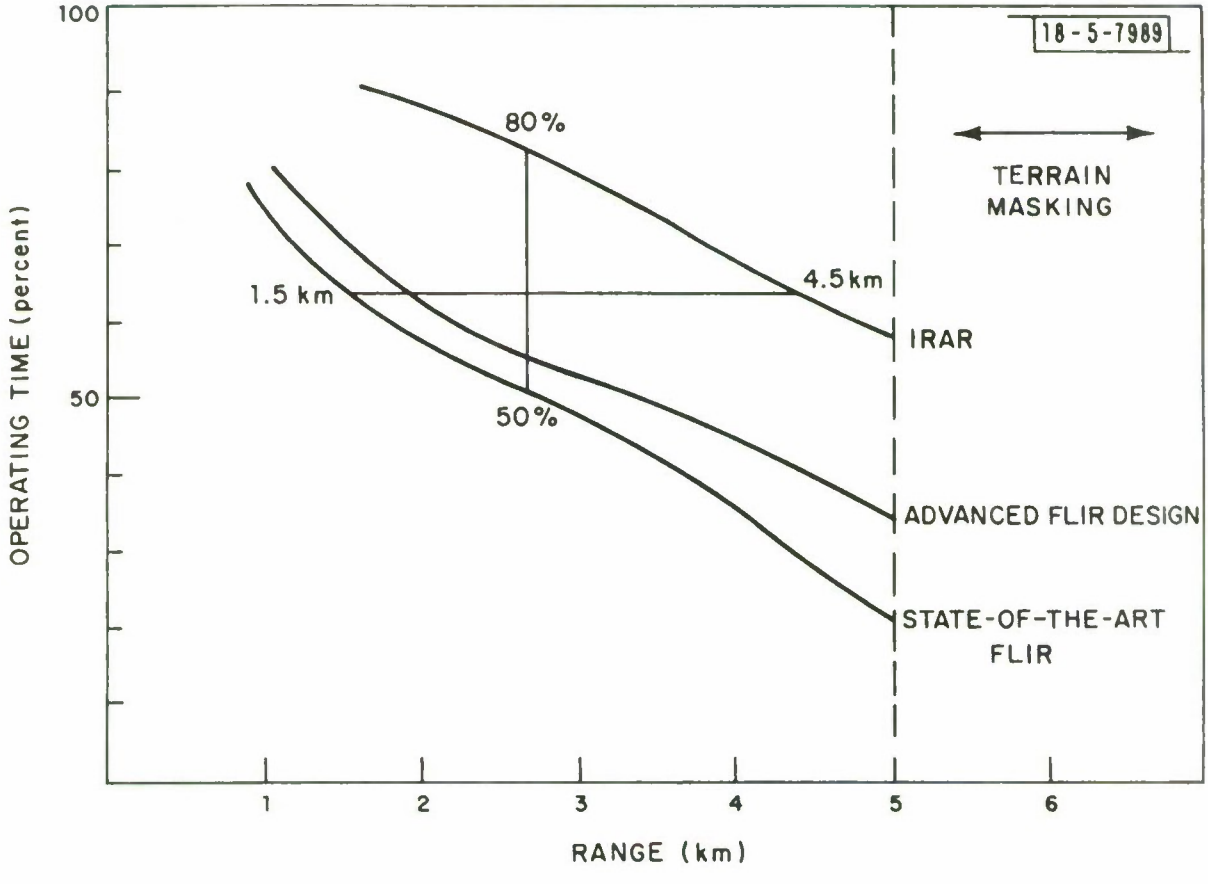

Fig. 17. Tactical sensor systems operational utility - winter.

There are several reasons for the superior weather performance of the infrared radar. First, the thermal signature of the target is limited by the physics of thermal emission processes while the active signature is based on the concentration of laser power on the appropriate resolution elements. Second, the active radar system uses heterodyne detection and so is not limited by background radiation. Third, a comparison of the dependence of SNR_p on angular resolution θ, including the θ dependence of the bandwidth B, as given by equations (14) and (16) will show that the FLIR system SNR_p is proportional to θ^6 while the IRAR SNR_p is proportional to θ^2. Improvement in angular resolution is therefore obtained at a high price in the FLIR system due to the severe relative reduction in SNR_p in comparison with that of the IRAR system. However, as shown in section II . the angular resolution of 0.05 mr is essential if these tactical sensors are to adequately perform the required target identification function.

IX. CONCLUSIONS

The principal conclusions of this design study are as follows.

1. A forward looking IR airborne radar can be expected to perform both of the target acquisition functions required for the short range tactical environment. These functions are (a) wide field MTI search and detection, and (b) narrow field high angular resolution recognition and identification.

2. In the MTI mode a 30° to 60° field-of-view can be searched at 5 km ahead of a Mach 0.5 aircraft with target detection down to 1 mph radial velocity threshold with probability of detection $P_D = 0.99$ and false alarm rate FAR = 4×10^{-4} sec^{-1}. The high angular resolution of the IR radar provides 27 dB signal processing gain through incoherent integration of multiple uncorrelated angular resolution cells in a single scan across a typical target.

3. Heterodyne array receiver techniques when combined with a 20 cm diameter aperture permit high resolution imaging with the required 8-13 angular resolution cells across the target minimum dimension at 30 frames/second. Local oscillator techniques described here meet the unique phase matching requirements for optical heterodyne operation of a detector array. One of these techniques, the holographic grating technique, also provides amplitude matching with a 3-4 dB additional improvement in signal-to-noise and a factor of 1.4-2.0 improvement in angular resolution.

4. Unambiguous ranging on any resolution cell within the field-of-view is available out to 5 km range at the typical pulsed laser PRF of 30 kHz when using a 16 element heterodyne array.

5. Design calculations show that there are at least three telescope configurations which will provide essentially aberration free performance over the required imaging field. These are:

   (a) an f/3 Ritchey-Chretien,

   (b) an f/1.5 Schmidt,

   (c) an f/1.5 Maksutov-Cassegrain.

   The f/1.5 Maksutov-Cassegrain has the advantage of compactness and the use of all spherical elements for reduced fabrication cost in quantity.

6. The main image processing issues are target speckle and target glints. Target speckle is reduced by frame averaging. Frame-to-frame angular decorrelation requirements associated with the aircraft altitude and speed are met at all frame rates up to 10^3 per second in essentially all tactical geometries. Target glints can be reduced by a nonlinear transformation of target reflectance to visual display brightness. The bidirectional reflectance design level for the IR radar translates directly into a target angular orientation design region for which this nonlinear transformation can be applied.

7. An IR airborne radar can be expected to have a weather penetration advantage of 25-30 dB over a FLIR of comparable size, weight, and cost.

This conclusion applies to a high quality state-of-the-art FLIR using 180 detectors and to an advanced generation FLIR design which would use a CCD or CID focal plane of 10^4 detector elements. As a result, in the winter in central Europe at a typical range of 2.5 km when the FLIR systems can be expected to penetrate the weather 50-55% of the time, the IR radar can be expected to penetrate the weather 80% of the time. Similarly, when the winter weather is such that it limits the FLIR systems to operating ranges between 1.5 and 2.0 km the IR radar can be expected to operate out to a range of 4.5 km.

ACKNOWLEDGEMENTS

Discussions with a number of individuals over a period of time have proved valuable in defining the system application and technology associated with an infrared airborne radar.

A. B. Gschwendtner and H. Kleiman have provided support and given me the benefit of their insight on a number of occasions.

R. J. Keyes played a central role in the initial investigation of the use of a CO_2 laser in a tactical infrared radar.

B. J. Berger and S. Marcus have developed a feasibility demonstration compact CO_2 laser radar which is now being used to obtain data.

R. H. Kingston has provided helpful comments regarding the heterodyne array mixing techniques described here.

REFERENCES

1. J. M. Lloyd, Thermal Imaging Systems (Plenum Press, New York, 1975).

2. M. I. Skolnik, Introduction to Radar Systems (McGraw-Hill, New York, 1962), chapters 3 and 4.

3. R. A. Rosell and R. H. Wilson in Perception of Displayed Information, edited by L. M. Biberman (Plenum Press, New York, 1973).

4. op cit, chapter 4.

5. A. E. Siegman, "The Antenna Properties of Optical Heterodyne Receivers", Proc. IEEE 54, 1350-1356 (1966).

6. J. J. Degnan and B. J. Klein, "Optical Antenna Gain 2: Receiving Antennas", Appl. Opt. 13, 2397-2401 (1974).

7. R. J. Becherer, "Angular Resolution and Signal-to-Noise Ratio of Imaging Infrared Radars", Lincoln Laboratory, M.I.T.(to be published).

8. Reference 2, p. 50-53.

9. M. Skolnik, Radar Handbook (McGraw-Hill, New York, 1970).

10. R. J. Keyes and T. M. Quist, "Low-Level Coherent and Incoherent Detection in the Infrared", in Semiconductors and Semimetals, Vol. 5, edited by R. K. Willardson and A. C. Beer (Academic Press, New York, 1970).

11. M. C. Teich, "Infrared Heterodyne Detection", Proc. IEEE 56, 37-46 (1968).

12. Reference 1, chapter 5.

13. Laser Speckle and Related Phenomena, edited by J. C. Dainty (Springer-Verlag, Berlin 1975).

14. Target Signature Analysis Center: Data Compilation, Eleventh Supplement, Vol. 1 - Bidirectional Reflectance: Definition, Discussion, and Utilization and Vol. 2 - Bidirectional Reflectance: Graphic Data p. 108, (1972). AFAL-TR-72-226.

15. A. P. Modica and H. Kleiman, "Statistics of Global IR Atmospheric Transmission", Project Report TT-7, Lincoln Laboratory, M.I.T. (3 March 1976). DDC AD-A024311/3.

UNCLASSIFIED

SECURITY CLASSIFICATION OF THIS PAGE *(When Data Entered)*

REPORT DOCUMENTATION PAGE		READ INSTRUCTIONS BEFORE COMPLETING FORM
1. REPORT NUMBER ESD-TR-77-271	2. GOVT ACCESSION NO.	3. RECIPIENT'S CATALOG NUMBER
4. TITLE *(and Subtitle)* System Design Study for Infrared Airborne Radar (IRAR)		5. TYPE OF REPORT & PERIOD COVERED Technical Note
		6. PERFORMING ORG. REPORT NUMBER Technical Note 1977-29
7. AUTHOR*(s)* Richard J. Becherer		8. CONTRACT OR GRANT NUMBER*(s)* F19628-78-C-0002
9. PERFORMING ORGANIZATION NAME AND ADDRESS Lincoln Laboratory, M.I.T. P.O. Box 73 Lexington, MA 02173		10. PROGRAM ELEMENT, PROJECT, TASK AREA & WORK UNIT NUMBERS Program Element No. 65705F Project No. 649L
11. CONTROLLING OFFICE NAME AND ADDRESS Air Force Systems Command, USAF Andrews AFB Washington, DC 20331		12. REPORT DATE 18 October 1977
		13. NUMBER OF PAGES 74
14. MONITORING AGENCY NAME & ADDRESS *(if different from Controlling Office)* Electronic Systems Division Hanscom AFB Bedford, MA 01731		15. SECURITY CLASS. *(of this report)* Unclassified
		15a. DECLASSIFICATION DOWNGRADING SCHEDULE

16. DISTRIBUTION STATEMENT *(of this Report)*

Approved for public release; distribution unlimited.

17. DISTRIBUTION STATEMENT *(of the abstract entered in Block 20, if different from Report)*

18. SUPPLEMENTARY NOTES

None

19. KEY WORDS *(Continue on reverse side if necessary and identify by block number)*

IRAR	narrow field	image processing
wide field	MTI detection	heterodyne detectors

20. ABSTRACT *(Continue on reverse side if necessary and identify by block number)*

This technical note describes the design of a tactical near-all-weather infrared airborne radar (IRAR). The requirements for this radar include both (1) wide field MTI search for target detection against a cluttered terrain background and (2) narrow field high angular resolution imagery for target recognition and identification.

The principal new technology issues identified and techniques proposed include a heterodyne detection antenna/receiver in an array configuration, compact Maksutov-Cassegrain telescope optics design, MTI pulse integration signal processing, and real time image processing for speckle and glint reduction.

Expected weather penetration capability for this radar is assessed with the aid of a recent analysis of real weather data from a number of locations in Central Europe.

DD FORM 1 JAN 73 1473 EDITION OF 1 NOV 65 IS OBSOLETE

UNCLASSIFIED

SECURITY CLASSIFICATION OF THIS PAGE *(When Data Entered)*